Argonne NATIONAL LABORATORY

ANL-10/13

Hydrogen Production by Water Dissociation Using Ceramic Membranes

Energy Systems Division

About Argonne National Laboratory

Argonne is a U.S. Department of Energy laboratory managed by UChicago Argonne, LLC under contract DE-AC02-06CH11357. The Laboratory's main facility is outside Chicago, at 9700 South Cass Avenue, Argonne, Illinois 60439. For information about Argonne and its pioneering science and technology programs, see www.anl.gov.

Availability of This Report

This report is available, at no cost, at http://www.osti.gov/bridge. It is also available on paper to the U.S. Department of Energy and its contractors, for a processing fee, from:

U.S. Department of Energy
Office of Scientific and Technical Information
P.O. Box 62
Oak Ridge, TN 37831-0062
phone (865) 576-8401
fax (865) 576-5728
reports@adonis.osti.gov

Disclaimer

This report was prepared as an account of work sponsored by an agency of the United States Government. Neither the United States Government nor any agency thereof, nor UChicago Argonne, LLC, nor any of their employees or officers, makes any warranty, express or implied, or assumes any legal liability or responsibility for the accuracy, completeness, or usefulness of any information, apparatus, product, or process disclosed, or represents that its use would not infringe privately owned rights. Reference herein to any specific commercial product, process, or service by trade name, trademark, manufacturer, or otherwise, does not necessarily constitute or imply its endorsement, recommendation, or favoring by the United States Government or any agency thereof. The views and opinions of document authors expressed herein do not necessarily state or reflect those of the United States Government or any agency thereof, Argonne National Laboratory, or UChicago Argonne, LLC.

ANL-10/13

Hydrogen Production by Water Dissociation Using Ceramic Membranes

prepared by
U. Balachandran, S.E. Dorris, J.E. Emerson, T.H. Lee,
Y. Lu, C.Y. Park, and J.J. Picciolo
Energy Systems Division, Argonne National Laboratory

February 23, 2010

HYDROGEN PRODUCTION BY WATER DISSOCIATION USING CERAMIC MEMBRANES

ANNUAL REPORT FOR FY 2009

ARGONNE NATIONAL LABORATORY
Energy Systems Division
9700 South Cass Avenue
Argonne, Illinois 60439

U. (Balu) Balachandran

Contributors:

S. E. Dorris
J. E. Emerson
T. H. Lee
Y. Lu
C.Y. Park
J. J. Picciolo

February 23, 2010

Work Supported by

U. S. DEPARTMENT OF ENERGY
Office of Fossil Energy, National Energy Technology Laboratory

Argonne National Laboratory is a U.S. Department of Energy laboratory managed by UChicago Argonne, LLC, under Contract Number DE-AC-02-06CH11357.

Contents

I. Objective 1

II. Highlights 1

III. Introduction 2

IV. Results 3

Milestone 1: Develop new membrane materials 3

Milestone 2: Fabricate/test thin-film OTM tubes using simulated coal combustion atmosphere to drive hydrogen production by water splitting. 16

Milestone 3: Test use of coal combustion atmosphere to drive hydrogen production by water splitting at low temperatures 25

V. Future Work 27

Publications and Presentations 28

References 30

Figures

1. Hydrogen production rates of thin-film and self-supporting SFT1 disks 4

2. Secondary electron image of ≈40-µm-thick SFT1 thin film on SFT1 substrate 5

3. Micrographs of $Sr_{0.95}Fe_{0.9}Ti_{0.1}O_x$ and $Sr_{0.97}Fe_{0.9}Ti_{0.1}O_x$ thin-film membranes sintered in air for 5-10 h at 1190°C. 6

4. Hydrogen production rates of Sr-deficient (SdFT1) and non-Sr-deficient (SFT1) disks 6

5. Hydrogen production rate of SdFT1 thin films and self-supported SFT1 disk at 900°C 7

6. Hydrogen production rates for $Sr_{0.95}$FT1 thin film and self-supporting SFT1 disk versus inverse temperature..... 8

7. SEM micrographs of $Sr_{0.95}$FT1 and $Sr_{0.97}$FT1 thin-films after hydrogen production measurements. 9

8. Surface micrograph of $Sr_{0.95}$FT1 thin film after hydrogen production rate measurements. 9

9. Secondary electron images (plan views) of SdFT1 disks sintered for 5 h in 100 ppm H_2/balance N_2 at a) 1200, b) 1250, and c) 1300°C. 11

10. Secondary electron images (plan views) of SdFT1 thin films sintered for 5 h in 100 ppm H_2/balance N_2 at a) 1200 and b) 1300°C. 11

11. Secondary electron images (plan views) of SFT1 disks sintered for 5 h in 100 ppm H_2/balance N_2 at a) 1200 and b) 1300°C..... 12

12. Hydrogen production rates for self-supporting SFN1 and SFT1 disks measured versus inverse temperature. 13

13. Hydrogen production rates at 900°C for SFT1-on-SFN1 and SdFT1-on-SFT1 samples measured vs. pH_2O on the hydrogen-generation side..... 14

14. Secondary electron images of SFT1 film on SFN1 substrate sintered 5 h at 1350°C in 100 ppm H_2/balance N_2..... 14

15. Hydrogen production rates versus inverse temperature for SFT1 thin film on SFN1 substrate and SFC2 film on SFC2 substrate 15

16. Secondary electron images of SFT1 thin films on SFN1 substrates sintered for 5 h in air at 1200and 1270°C..... 16

17. Spring-loaded fixture for measuring hydrogen production rate. 17

18. Hydrogen production rate of SFC2 tube at 900°C versus pH_2O on hydrogen-generation side 18

19. Hydrogen production rate of SFC2 tube vs. inverse temperature 19

20. Hydrogen production rate vs. pH_2O on hydrogen-generation side of SFC2 tube at 900°C 20

21. Thin-film SFC2 tube made by paste-painting technique 20

22. Hydrogen production rate vs. temperature for thin-film and self-supported SFC2 tubes 21

23. Hydrogen production rate at 900°C vs. pH_2O on steam side of thin-film and self-supported SFC2 tubes 22

24. Hydrogen production rate of thin-film SFC2 tube vs. flow rate of humidified N_2 on steam side of tube 23

25. Secondary electron image of LSCF7328 thin-film tube that was tested using reducing gas to drive hydrogen production via water dissociation 24

26. Hydrogen production rate at 600-900°C for LSCF7328 thin film on porous LSCF7328 substrate vs. CO concentration in gas on oxygen-permeate side 26

27. Hydrogen production rate of LSCF7328 thin film on porous LSCF7328 substrate versus inverse temperature using various CO/CO_2 gas mixtures on oxygen-permeate side 27

Tables

1. Effect of gas flow rates on hydrogen production rate of tubular SFC2 thin film 23

HYDROGEN PRODUCTION BY WATER DISSOCIATION USING CERAMIC MEMBRANES

ANNUAL REPORT FOR FY 2009

ARGONNE NATIONAL LABORATORY

Project Title: Hydrogen Production by Water Dissociation using Ceramic Membranes

NETL Project Manager: Richard Dunst

ANL Project PI: U. (Balu) Balachandran

B&R Code/Contract Number: AA-10-40-00-00-0/FWP 49347

Report Date: February 23, 2010

I. OBJECTIVE

The objective of this project is to develop dense ceramic membranes that can produce hydrogen via coal/coal gas-assisted water dissociation without using an external power supply or circuitry.

II. HIGHLIGHTS

1. Low hydrogen production rates of Sr-deficient $Sr_{1.0}Fe_{0.9}Ti_{0.1}O_x$ (SdFT1) thin films were attributed to decomposition of SdFT1 materials sintered at temperatures below 1300°C, as indicated by the presence of needle-like grains in samples.

2. A new OTM material, $SrFe_{0.9}Nb_{0.1}O_{3-\delta}$ (SFN1), shows promise as a substrate for $Sr_{1.0}Fe_{0.9}Ti_{0.1}O_x$ (SFT1) thin films, because it does not densify as completely as SFT1 and maintains sufficient porosity during sintering.

3. The hydrogen production rate of SFT1 thin films was increased significantly by producing single-phase material on an SFN1 substrate.

4. The hydrogen production rates of OTM tubes were measured in tests using simulated coal combustion products to drive water splitting.

5. The principle of using coal combustion products to drive hydrogen production by water splitting was demonstrated in tests using CO/CO_2 mixtures at 600-900°C with $La_{0.7}Sr_{0.3}Cu_{0.2}Fe_{0.8}O_{3-\delta}$ (LSCF7328) thin films on a LSCF7328 substrate.

III. INTRODUCTION

This project grew from an effort to develop a dense ceramic membrane for separating hydrogen from gas mixtures such as those generated during coal gasification, methane partial oxidation, and water-gas shift reactions [1]. That effort led to the development of various cermet (i.e., ceramic/metal composite) membranes that enable hydrogen production by two methods. In one method, a hydrogen transport membrane selectively removes hydrogen from a gas mixture by transporting it through either a mixed protonic/electronic conductor or a hydrogen transport metal. In the other method, an oxygen transport membrane (OTM) generates hydrogen mixed with steam by removing oxygen that is generated through water splitting [1, 2].

This project focuses on the development of OTMs that efficiently produce hydrogen via the dissociation of water. Supercritical boilers offer very high-pressure steam that can be decomposed to provide pure hydrogen by means of OTMs. Oxygen resulting from the dissociation of steam can be used for coal gasification, enriched combustion, or synthesis gas production. Hydrogen and sequestration-ready CO_2 can be produced from coal and steam by using the membrane being developed in this project. Although hydrogen can also be generated by high-temperature steam electrolysis, producing hydrogen by water splitting with a mixed-conducting membrane requires no electric power or electrical circuitry.

Water dissociates into oxygen and hydrogen at high temperatures by the reaction:

$$H_2O(g) \Leftrightarrow H_2 + \frac{1}{2}O_2$$

However, very low concentrations of hydrogen and oxygen are generated even at relatively high temperatures (e.g., 0.1 and 0.042% for hydrogen and oxygen, respectively, at 1600°C), because the equilibrium constant for the reaction is small [3]. This shortcoming can be overcome at moderate temperatures by using a mixed-conducting (electron- and ion-conducting) membrane to remove either oxygen or hydrogen, which shifts the equilibrium toward dissociation. If an OTM is used to produce hydrogen, the hydrogen production rate depends directly on the rate at which oxygen is removed from the water dissociation zone, which depends on the OTM's oxygen permeability (a function of the OTM's electron and oxygen-ion conductivities), the surface oxygen exchange kinetics, and the oxygen partial pressure (pO_2) gradient across the OTM [4-7]. To obtain a high hydrogen production rate, mixed-conducting OTMs should exhibit high electron and oxygen-ion conductivities, possess good surface exchange properties, and be exposed to a high pO_2 gradient.

Others have used mixed-conducting OTMs to produce hydrogen by water dissociation, but the membranes had low electronic conductivity, and the hydrogen production rate was modest even at high temperature, e.g., 0.6 cm^3 (STP)/min-cm^2 at 1683°C [8]. We achieved a significantly higher hydrogen production rate by using an OTM composed of an oxygen-ion conductor of cerium gadolinium oxide (CGO) and an

electronic conductor (Ni) [2]. The hydrogen production rate increased with increases in temperature, water partial pressure on the hydrogen-production side of the membrane, and oxygen chemical potential gradient across the membrane [2]. It also increased with decreasing membrane thickness, but it became limited by surface reaction kinetics for OTMs with thickness < ≈0.5 mm.

To be practical for hydrogen production, OTMs must give high hydrogen production rates and be available in a shape with a large active area, e.g., tubes. The OTMs must also remain chemically and mechanically stable in corrosive environments at elevated temperatures. All experimental milestones for FY 2009 were met in tests using OTMs that were developed at Argonne. This report summarizes progress during FY 2009 toward the fabrication of practical OTMs. The following milestones were established in the Field Work Proposal for FY 2009 as benchmarks in developing practical OTMs:

1. Develop new membrane materials.
2. Fabricate and test thin-film OTM tubes using simulated coal combustion atmosphere to drive hydrogen production by water splitting.
3. Test use of coal combustion atmosphere to drive hydrogen production by water splitting at low temperatures.

IV. RESULTS

Results are presented below in relation to the pertinent milestone for FY 2009.

Milestone 1. Continue to develop new membrane materials.

A 25-μm-thick $SrFeCo_{0.5}O_x$ (SFC2) film on a porous SFC2 substrate gave the highest hydrogen production rate to date for an Argonne OTM, 17.4 cm^3/min-cm^2 [9], but SFC2 undergoes a phase transition that dramatically reduces its hydrogen production rate at low temperatures (<825°C). To increase hydrogen production rates at low temperatures, we are investigating several promising alternative OTM compositions, such as $La_{0.7}Sr_{0.3}Cu_{0.2}Fe_{0.8}O_{3-\delta}$ (LSCF7328) and compositions in the Sr-Fe-Ti-O (SFT) system. We showed [9] that coating the surfaces of LSCF7328 membranes increases their hydrogen production rate, and our tests of these membranes using CO/CO_2 gas mixtures demonstrated that coal combustion can be used to drive the production of hydrogen via water dissociation. We are also testing SFT membranes for low-temperature applications. Because Sr deficiency increases the stability of SFT in humidified atmospheres [10], we are investigating the effect of this deficiency on the hydrogen production rate under water splitting conditions. This report describes the progress made during FY 2009 toward fabricating OTMs from LSCF7328 and compositions in the SFT system.

Thin films of $Sr_{1.0}Fe_{0.9}Ti_{0.1}O_x$ (SFT1) and Sr-deficient SFT1 (SdFT1) were made on porous substrates. The substrates were prepared from a powder mixture made by mixing the corresponding OTM composition with 20 wt.% carbon. The mixture was uniaxially pressed (2,000 atm, 200 MPa) into a disk and pre-sintered in air for 5 h at 950°C to remove the carbon and provide the disk with mechanical integrity. Thin films were made

by casting a dispersion of OTM powder onto a substrate of the same composition and sintering for 5-10 h at 1190-1330°C in an atmosphere of air or ≈100 ppm H_2/balance N_2. Self-supporting disks were prepared by uniaxially pressing (2,000 atm, 200 MPa) SFT1 and SdFT1 powders and then sintering in an atmosphere of ≈100 ppm H_2/balance N_2 at 1330°C for 5 h.

The SFT1 and SdFT1 samples were sealed to an Al_2O_3 tube by using an assembly described elsewhere [11], and the hydrogen production rate was measured. During the measurements, N_2 was bubbled through water whose temperature was adjusted to give a water partial pressure (pH_2O) of 0.49 atm. Humidified N_2 was flowed over one side of the membrane, called the hydrogen-generation side, while 80% H_2/balance He was flowed over the other side, called the oxygen-permeate side. Hydrogen fixed a low pO_2 on the oxygen-permeate side and established a pO_2 gradient by reacting with oxygen that diffused through the OTM. The H_2/He mixture served as a model gas to evaluate the effects of membrane thickness and composition on hydrogen production rate. A Hewlett-Packard 6890 gas chromatograph was used to measure H_2 concentrations in the gas stream at temperatures of 600-900°C. The microstructures of samples were examined with a scanning electron microscope (JEOL JSM-5400).

Figure 1 plots the the hydrogen production rates of a ≈40-µm-thick SFT1 film and a 1.1-mm-thick self-supporting SFT1 disk versus inverse temperature. The hydrogen production rate of the thin-film sample is higher than that of the much thicker self-supporting disk at lower temperature but is much lower overall than is expected based on the film's thickness. Figure 2 shows a secondary electron image of the thin-film sample taken after its hydrogen production rate was measured.

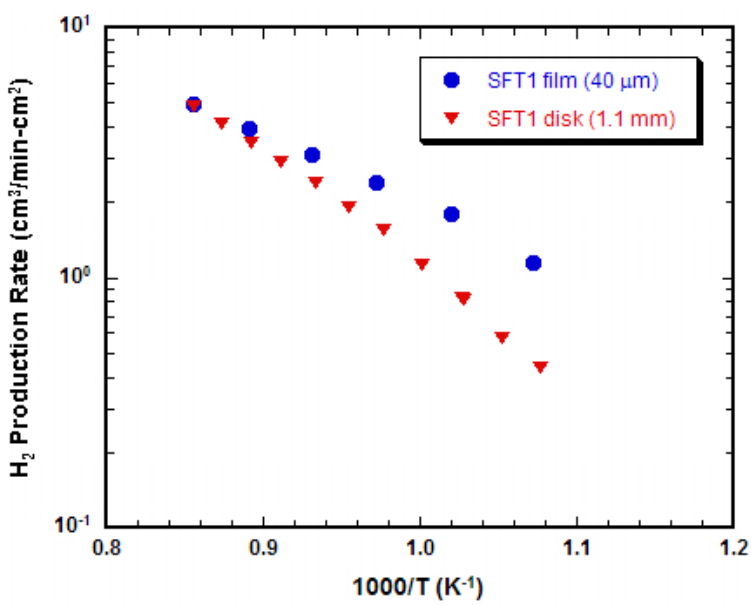

Fig. 1 Hydrogen production rates of thin-film and self-supporting SFT1 disks, measured with humidified N_2 (pH_2O = 0.49 atm) on water-splitting side and 80% H_2/balance He on oxygen-permeate side. Sample thickness is given in parentheses in inset.

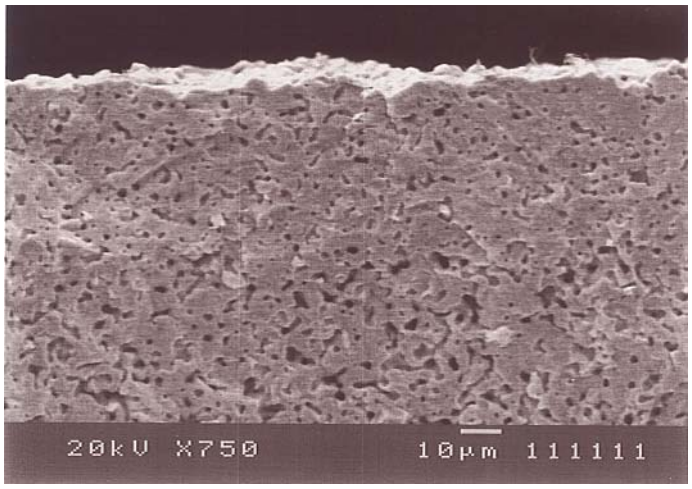

Fig. 2 Secondary electron image of ≈40-μm-thick SFT1 thin film on SFT1 substrate showing no clear boundary between thin film at top and substrate below.

The low hydrogen production rate for the thin-film sample might be related to an unfavorable microstructure. Rather than a clear demarcation between a dense thin film and a porous substrate, the sample appeared to have uniform density across its thickness. Isopropyl alcohol (IPA) applied to one surface did not penetrate the sample, even though considerable porosity was evident in both the substrate and the thin film. The lack of IPA penetration indicates that the porosity was not interconnected from one surface of the sample to the other. The uniform density across the sample's thickness suggests that the interconnection of pores was sparse in both the substrate and the thin film. Insufficient interconnected porosity in the substrate hinders gas transport, in general, and might explain the lower-than-expected hydrogen production rate of the thin film sample. To increase the hydrogen production rate, porosity should be increased in the substrate by either lowering the sintering temperature or increasing the amount of pore former in the substrate. If a lower sintering temperature is required, high density can be maintained in the thin film by modifying the film's composition, by using fine-grain SFT powder, or by adding a sintering aid to the film.

Strontium-deficient-SFT1 compositions ($Sr_{0.95}Fe_{0.9}Ti_{0.1}O_x$ and $Sr_{0.97}Fe_{0.9}Ti_{0.1}O_x$) are being investigated, because they sinter more easily than SFT1 membranes [9], and Sr deficiency might enhance the stability of SFT in humidified atmospheres [10]. The SdFT1 thin films on porous substrates of the same composition were sintered in an atmosphere of either air or 100 ppm H_2/balance N_2. Films sintered in 100 ppm H_2/balance N_2 tended to develop multiple small cracks, i.e., "mud cracks," when they were tested for IPA penetration. In contrast, samples sintered in air did not crack and densified below the sintering temperature (1330°C) for SFT1 thin films. Figure 3 shows secondary electron images of $Sr_{0.95}Fe_{0.9}Ti_{0.1}O_x$ and $Sr_{0.97}Fe_{0.9}Ti_{0.1}O_x$ films sintered in air at 1190°C. Both SdFT1 films appear denser than the SFT1 film and, unlike the SFT1 sample (Fig. 2), they exhibit a clear boundary between a dense thin film that is necessary to produce hydrogen with high purity and a porous substrate that is required to produce hydrogen rapidly.

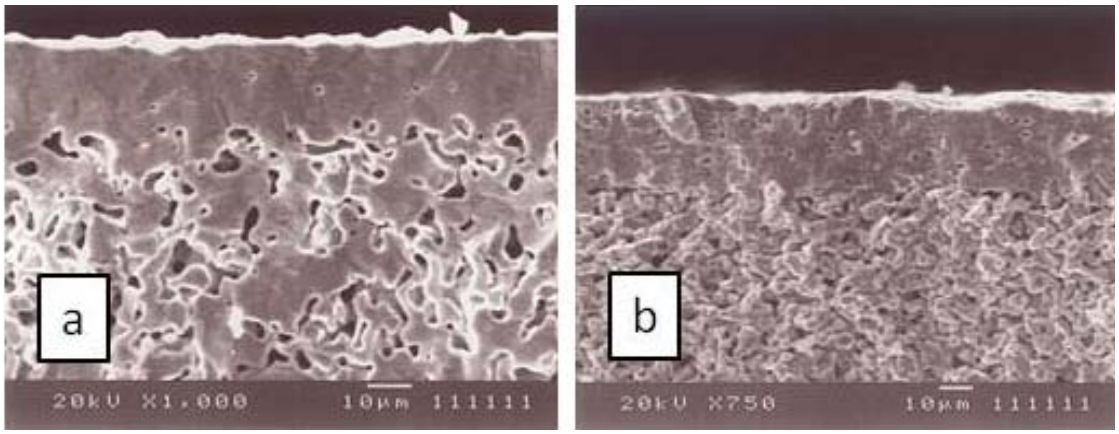

Fig. 3 Micrographs of a) $Sr_{0.95}Fe_{0.9}Ti_{0.1}O_x$ and b) $Sr_{0.97}Fe_{0.9}Ti_{0.1}O_x$ thin-film membranes sintered in air for 5-10 h at 1190°C.

To further study the effect of Sr deficiency, we measured the hydrogen production rates of membranes with compositions of $Sr_{0.95}Fe_{0.9}Ti_{0.1}O_x$, $Sr_{0.97}Fe_{0.9}Ti_{0.1}O_x$, and SFT1. The hydrogen production rate of self-supporting disks (thickness ≈1 mm) was measured in the temperature range 700-900°C. The results, shown in Fig. 4, were obtained while flowing humidified N_2 (pH_2O = 0.49 atm) over the water-splitting side of the disks and 80% H_2/balance He over the oxygen-permeate side. The hydrogen production rate for both Sr-deficient membranes is slightly lower than that of the non-Sr-deficient (SFT1) membrane. The apparent activation energy is similar for both Sr-deficient membranes, but is slightly higher that that for SFT1. Although the hydrogen production rates of the SdFT1 membranes are slightly lower than those of SFT1, their superior sintering properties might compensate for their inferior hydrogen production rates by facilitating the fabrication of dense thin films.

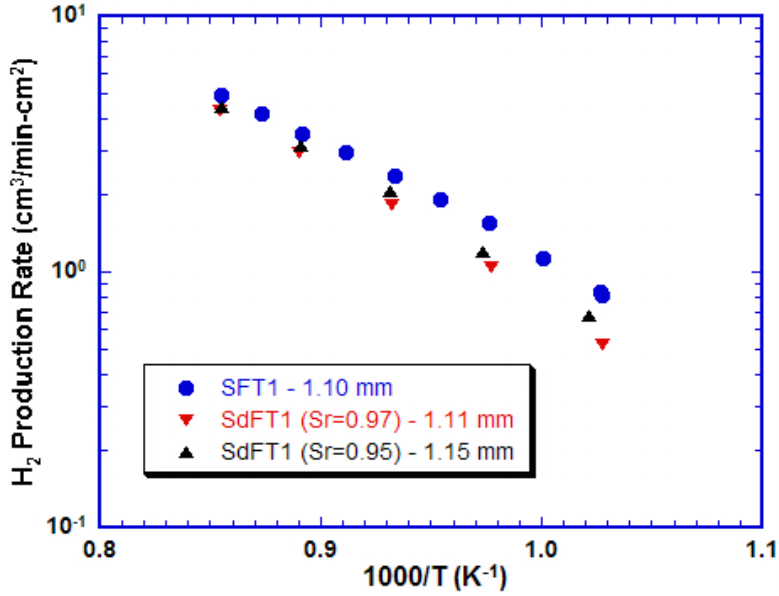

Fig. 4 Hydrogen production rates of self-supporting Sr-deficient (SdFT1) and non-Sr-deficient (SFT1) disks measured with humidified N_2 (pH_2O = 0.49 atm) on water-splitting side and 80% H_2/balance He on oxygen-permeate side.

Figure 5 shows the hydrogen production rate of ≈20-µm-thick SdFT1 films measured at 900°C. The $Sr_{0.95}$FT1-A film was sintered for 5 h in 100 ppm H_2/balance N_2 at 1180°C, while $Sr_{0.95}$FT1-B and $Sr_{0.97}$FT1 films were sintered for 12 h in air at 1160°C. The hydrogen production rate of a self-supported, 1.1-mm-thick SFT1 membrane is shown for comparison. The hydrogen production rate was measured as a function of pH_2O (0.03-0.49 atm) on the water-splitting side of membranes with 80% H_2/balance He on the oxygen-permeate side. For all of the membranes, the hydrogen production rate increased as pH_2O increased.

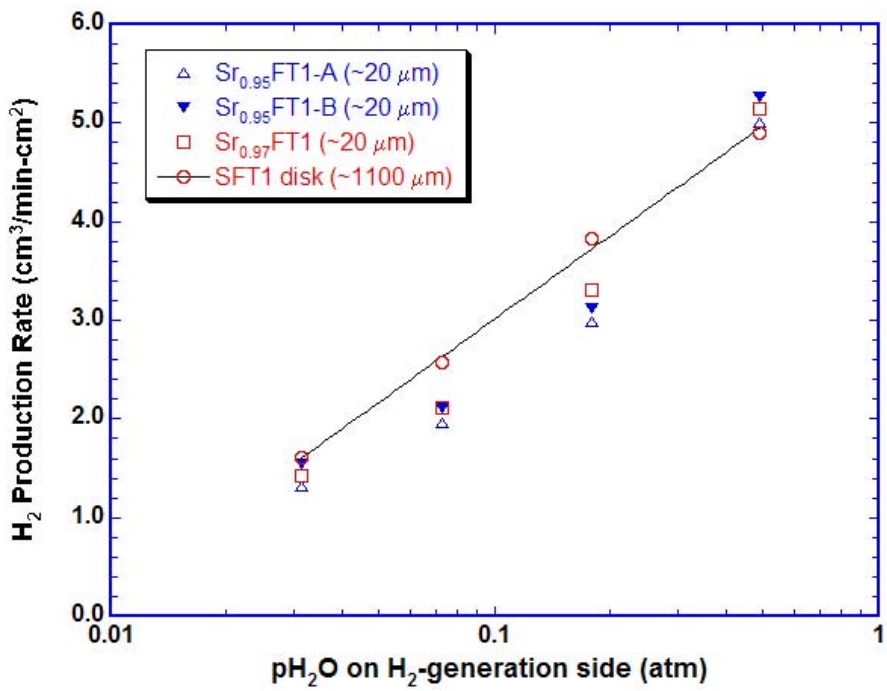

Fig. 5 Hydrogen production rate of SdFT1 films and self-supported SFT1 disk at 900°C with 80% H_2/balance He on the oxygen-permeate side and wet N_2 on hydrogen-generation side. Inset gives membrane thickness.

Regardless of membrane thickness (Fig. 5 inset) and sintering condition, the three thin-film membranes gave similar hydrogen production rates. Surprisingly, the hydrogen production rate of the self-supported disk is higher than that of the much thinner film membranes at low pH_2O, and is only slightly lower at pH_2O = 0.49 atm. The hydrogen production rate of the self-supported disk showed a logarithmic dependence on pH_2O, but the hydrogen production rates of the thin-film samples did not. The deviation from logarithmic dependence on pH_2O may indicate that the hydrogen production rate of thin films is mainly limited by slow surface kinetics of oxygen exchange, which could result from concentration polarization due to insufficient porosity in the substrate or from the inherent surface exchange properties of the films. The observation that membrane thickness was not a factor also suggests that surface phenomena might be controlling the hydrogen production rate.

Figure 6 shows the temperature dependence of hydrogen production rate for the $Sr_{0.95}FT1$-A thin film and the self-supporting SFT1 disk. The hydrogen production rate was measured with pH_2O = 0.49 atm on the hydrogen-generation side of the samples and 80% H_2/balance He on the oxygen-permeate side. As shown in Fig. 6, the hydrogen production rate of the thin film was only slightly higher than that of the self-supporting membrane, even though its thickness was much smaller (≈20 μm vs. ≈1100 μm). Thus, membrane thickness had little effect on the hydrogen production rate.

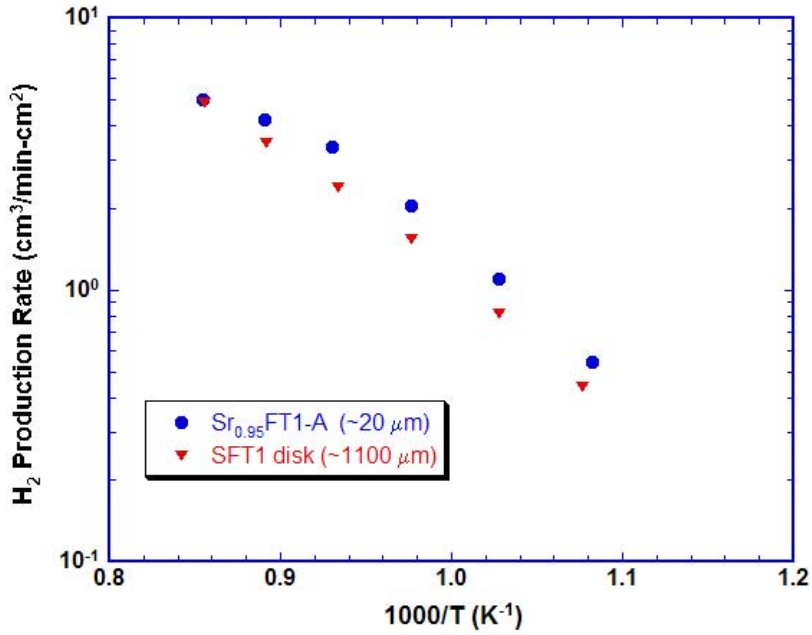

Fig. 6 Hydrogen production rates for $Sr_{0.95}FT1$-A thin film and self-supporting SFT1 disk, measured with N_2 (pH_2O=0.49 atm) on hydrogen-generation side and 80% H_2/balance He on oxygen-permeate side.

After the hydrogen production measurements, the substrate porosity and thin-film density were examined by scanning electron microscopy (SEM). Figure 7 shows the fracture surfaces of the $Sr_{0.95}FT1$-A, $Sr_{0.95}FT1$-B, and $Sr_{0.97}FT1$ thin-film samples. All the films appeared dense, with only isolated porosity and a film thickness of ≈20 μm on a porous SFT1 substrate. Before the samples were installed in the reactor, IPA-penetration tests confirmed that the thin films were dense. The porosity in the substrates appeared to be uniformly distributed and adequate for gas diffusion; therefore, it seems unlikely that the substrates caused the low hydrogen production rates of the thin-film samples.

An alternative explanation for the low hydrogen production rates of thin-film samples is suggested by a plan-view micrograph taken of the $Sr_{0.95}FT1$-A film after the hydrogen production measurements (Fig. 8). The surface shows at least two types of grain: big, round grains and small, needle-shaped grains. This microstructure (sample sintered at 1180°C) was not seen on the surface of samples that were sintered at higher temperature (1330°C). This difference in microstructures suggests that the low hydrogen production rate of thin films may be related to the presence of a second phase.

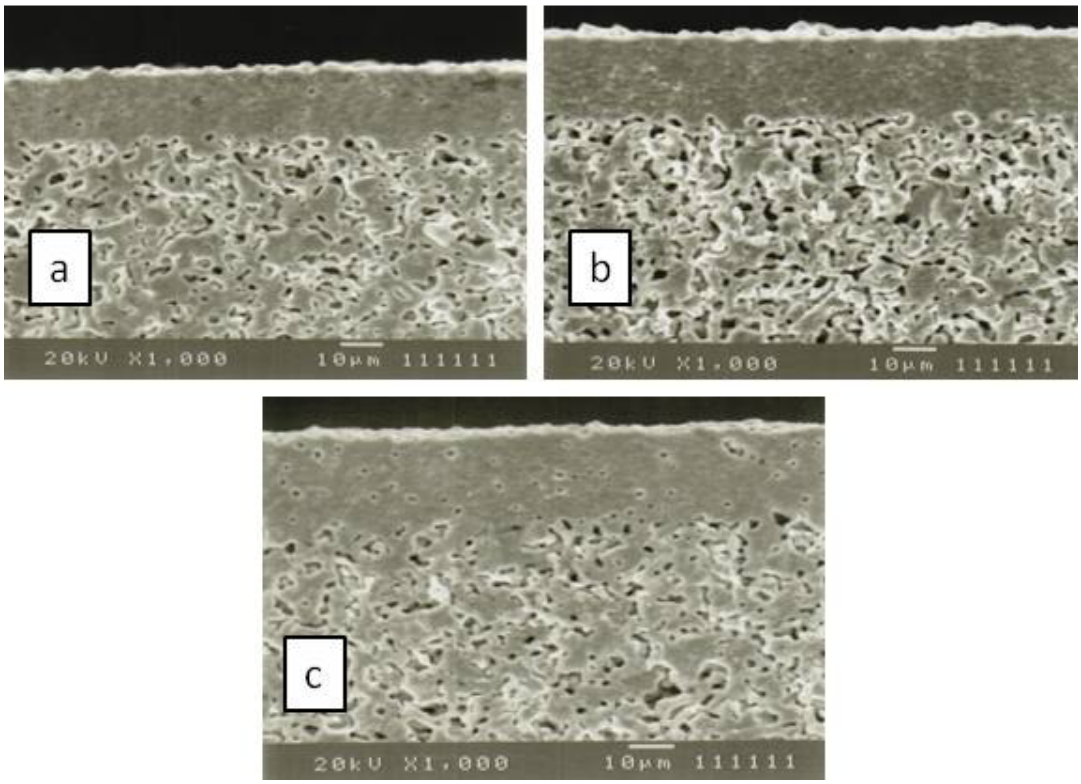

Fig. 7 Micrographs of a) $Sr_{0.95}FT1$-A, b) $Sr_{0.95}FT1$-B, and c) $Sr_{0.97}FT1$ thin-film membranes after hydrogen production measurements.

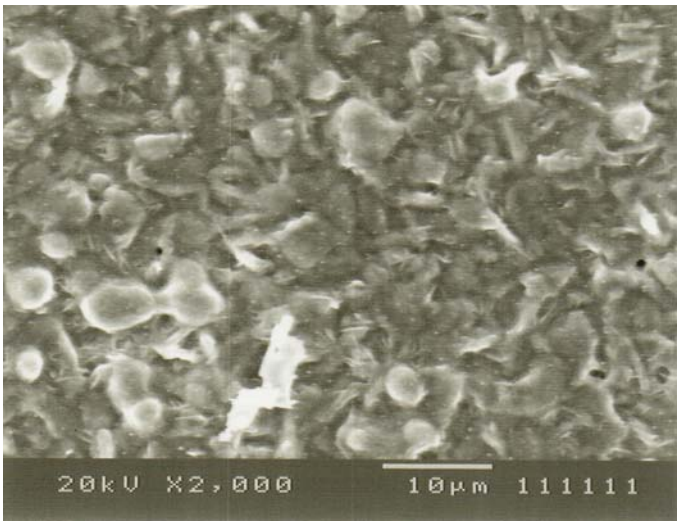

Fig. 8 Surface micrograph of $Sr_{0.95}FT1$-A film taken after hydrogen production rate measurements.

To efficiently produce high-purity hydrogen by water splitting, thin-film OTMs must contain a thin, dense layer without interconnected porosity on a substrate with sufficient porosity to allow rapid gas transport to and from the dense layer. The hydrogen production rates for SFT thin films (Fig. 1) and SdFT thin films (Fig. 5) were lower than expected due to difficulty producing both a porous substrate and a dense thin film.

Sintering at temperatures high enough to produce dense SFT1 thin films left insufficient porosity in SFT1 substrates, while sufficient porosity was obtained with SdFT1 thin films that densified at lower sintering temperatures, but a second phase inhibited hydrogen production. To avoid these problems, single-phase SFT1 thin films were made on substrates composed of $SrFe_{0.9}Nb_{0.1}O_{3-\delta}$ (SFN1), an OTM material that does not densify as readily as SFT1 and maintains sufficient porosity after sintering.

Powders of SFT1, SdFT1, and SFN1 were prepared by conventional solid-state reaction among their constituent oxides. The SFT1 and SdFT1 were made from mixtures of $SrCO_3$, Fe_2O_3, and TiO_2 powders; and the SFN1, from a mixture of $SrCO_3$, Fe_2O_3, and Nb_2O_5 powders. The mixtures were milled in isopropyl alcohol for 24 h with zirconia media, and then dried over a hot plate. The dried powder mixture was calcined in ambient air at 850°C for 12 h. The powder was milled and calcined again for 12 h in ambient air at 900°C and then was milled a third time before further processing. Self-supporting membrane disks were made by uniaxially pressing milled powder and sintering for 10 h in 100 ppm H_2/balance N_2 at 1200-1350°C.

We fabricated thin films of SFT1 on porous SFN1 substrates and $Sr_{0.95}Fe_{0.9}Ti_{0.1}O_x$ (SdFT1) on porous SFT1 substrates. The substrates were made by uniaxially pressing (2,000 atm, 200 MPa) disk-shape specimens from mixtures of carbon (20 wt.%) and either SFT1 or SFN1 powder. The disks were pre-sintered in ambient air for 5-10 h at 950-1050°C to remove the carbon and provide the disks with mechanical integrity. Thin films were made by casting a dispersion of SFT1 or SdFT1 powder onto a pre-sintered substrate. The SFT1 thin films were sintered for 5-10 h at ≈1350°C in an atmosphere of 100 ppm H_2/balance N_2 or ambient air. The SdFT1 thin films were sintered for 5-10 h at ≈1170°C in an atmosphere of 100 ppm H_2/balance N_2 or ambient air. Before they were cooled to room temperature, the thin films were annealed for 5 h at 700°C.

Sintering temperature markedly affects the microstructure of SdFT1 samples but not that of SFT1 samples. Figure 9 shows micrographs taken from as-sintered surfaces of SdFT1 disks sintered for 5 h at 1200-1300°C in 100 ppm H_2/balance N_2. Samples sintered at either 1200 or 1250°C contained rounded grains and a second phase with needle-shaped grains, but a disk sintered at 1300°C exhibited only rounded grains. Likewise, an SdFT1 film sintered at 1200°C showed the needle-shaped second phase and rounded grains (Fig. 10a), but one sintered at 1300°C had only rounded grains (Fig. 10b). In contrast, as-sintered SFT1 disks showed only rounded grains after sintering for 5 h in 100 ppm H_2/balance N_2 at either 1200°C (Fig. 11a) or 1300°C (Fig. 11b). Needlelike grains were evident in SdFT1 samples sintered at ≤1250°C, but were not seen in SdFT1 samples sintered at higher temperatures or in SFT1 samples sintered under the same conditions. The appearance of needlelike grains in SdFT1, but not SFT1, samples suggests that SdFT1 samples are less stable at <1300°C and must be sintered at ≥1300°C to obtain single-phase material.

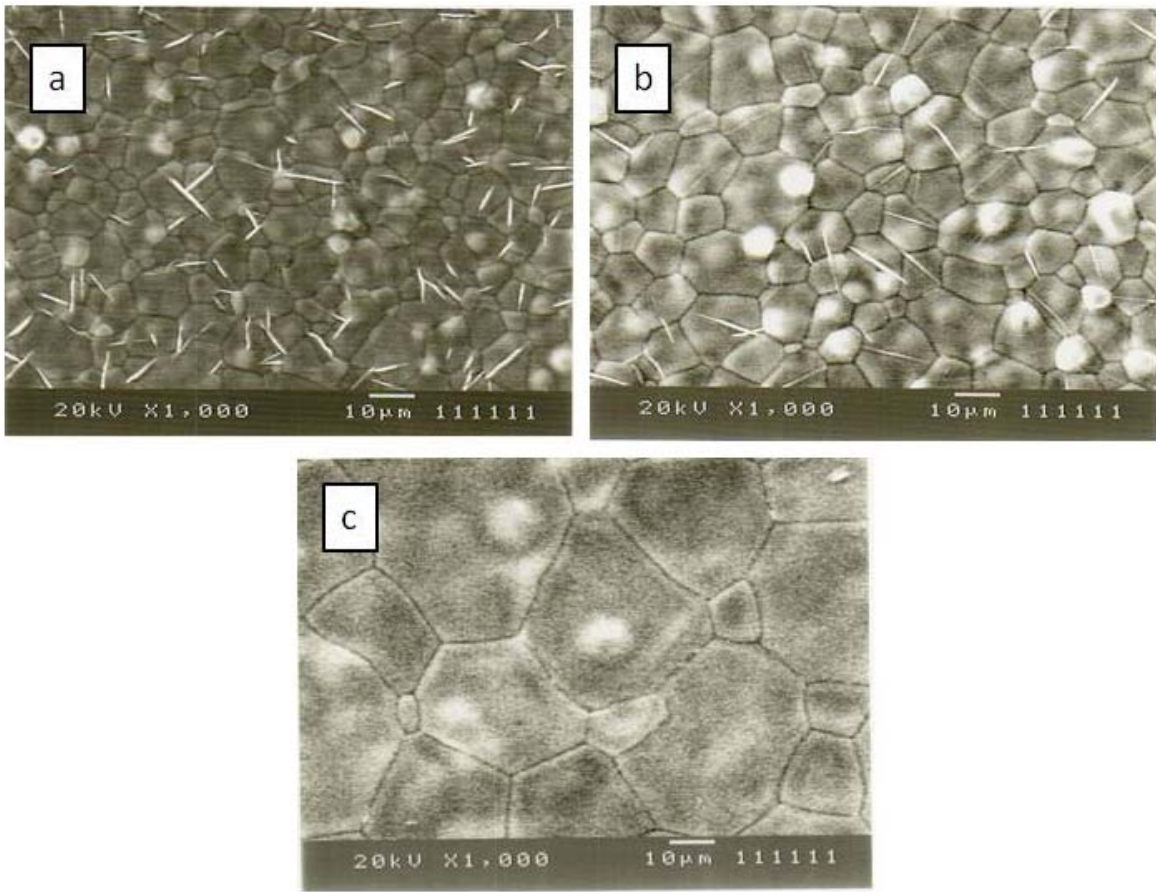

Fig. 9 Secondary electron images (plan views) of SdFT1 disks sintered for 5 h in 100 ppm H_2/balance N_2 at a) 1200, b) 1250, and c) 1300°C.

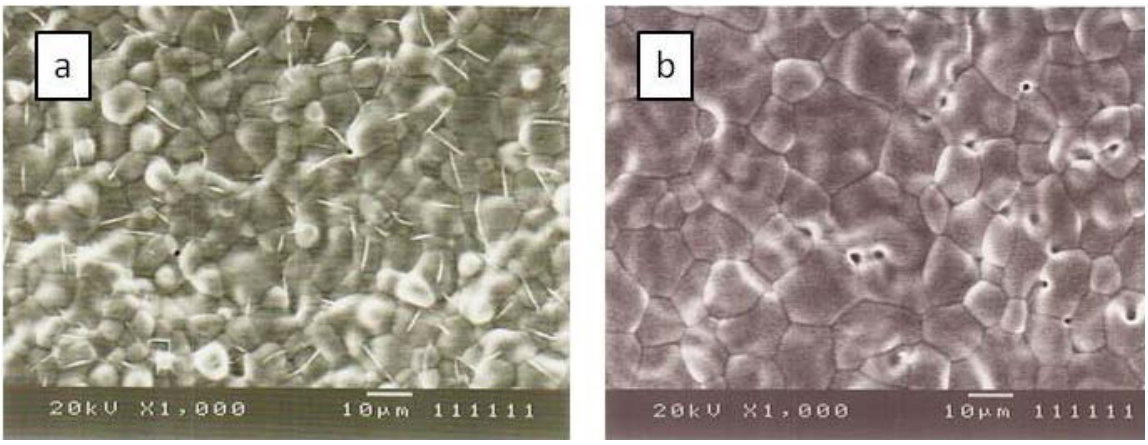

Fig. 10 Secondary electron images (plan views) of SdFT1 thin films sintered in 100 ppm H_2/balance N_2 for 5 h at a) 1200 and b) 1300°C. Films were made on SFT1 substrates.

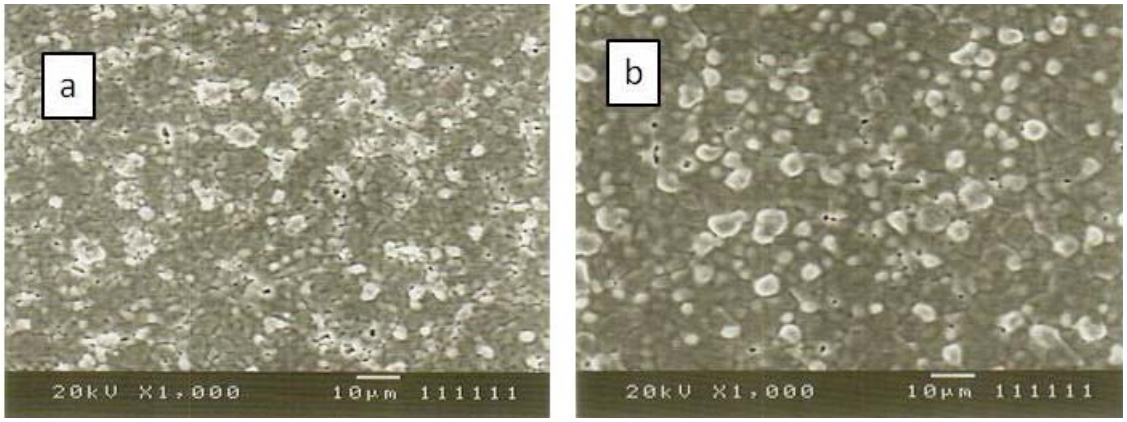

Fig. 11 Secondary electron images (plan views) of SFT1 disks sintered in 100 ppm H_2/balance N_2 for 5 h at a) 1200 and b) 1300°C.

Correlating the microstructures of SdFT1 samples (Fig. 10) with their sintering temperature and hydrogen production rates revealed that samples with needle-like grains give much lower hydrogen production rates than samples without them. Though not confirmed with SEM, SdFT1 and SFT1 disks sintered at 1330°C should be free of needle-like grains due to their sintering temperature, and their hydrogen production rates are approximately equivalent (Fig. 4). On the other hand, an SdFT1 thin film sintered at 1180°C was seen to contain needle-shaped grains, and its hydrogen production rate was only slightly higher than that of an SFT1 disk, even though the SdFT1 film was much thinner (≈20 μm vs. ≈1100 μm) (Fig. 6). Although high hydrogen production rates are obtained with SdFT1 samples sintered at high temperature (>1300°C), the presence of the second phase in samples sintered at lower temperatures and its effect on the hydrogen production rate suggest that chemical instability might be problematic for SdFT1 membranes used at lower temperature. The correlation between microstructure and hydrogen production rate indicates that SdFT1 thin films must be sintered at high temperature (>1300°C) to prevent formation of the needle-shaped second phase and achieve a high hydrogen production rate; therefore, reducing the sintering temperature by using SdFT1 thin films is not a practical way to increase porosity in SFT1 substrates.

In another approach for producing a substrate with adequate porosity, we are testing SFN1 as an alternative substrate material. Figure 12 compares the temperature dependence of the hydrogen production rate for self-supporting SFN1 and SFT1 disks with thickness of ≈1 mm. The hydrogen production rate was measured with pH_2O = 0.49 atm on the hydrogen-generation side and 80% H_2/balance He on the oxygen-permeate side. The hydrogen production rate of SFN1 is only slightly lower than that of SFT1, and its apparent activation energy is similar to that of SFT1. Like SFT1 membranes, SFN1 samples do not exhibit an abrupt change in hydrogen production rate like that associated with the phase transition in SFC2 membranes [12]. With a high hydrogen production rate and an expected high sintering temperature, SFN1 was tested as a substrate material for SFT1 thin films. Although the SFT1 thin film and SFN1 substrate might exhibit some solid solubility during sintering, the similarity in their hydrogen production rates suggests that the hydrogen production rate should not be degraded.

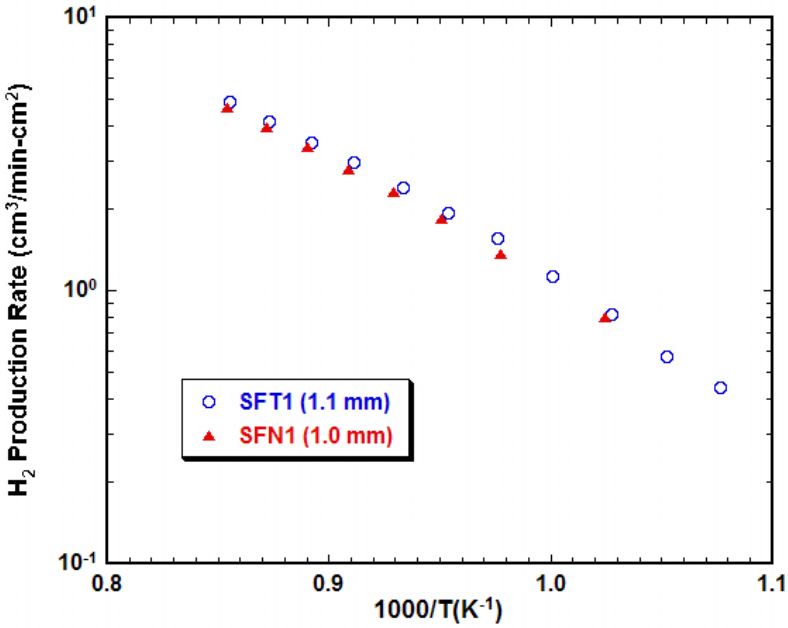

Fig. 12 Hydrogen production rates for SFN1 and SFT1 disks measured with 80% H_2/balance He on oxygen-permeate side and humidified N_2 (pH_2O = 0.49 atm) on hydrogen-generation side. Inset gives membrane thickness.

Figure 13 shows the hydrogen production rate of an SFT1 thin film on an SFN1 substrate. The film was sintered for 5 h at 1350°C in 100 ppm H_2/balance N_2 and had a thickness of ≈30 µm. The hydrogen production rate of an SdFT1 film (thickness ≈20 µm) on an SFT1 substrate is shown for comparison. The hydrogen production rate was measured as a function of pH_2O (0.03-0.49 atm) in N_2 on the hydrogen-generation side while 80% H_2/balance He flowed on the oxygen-permeate side. The hydrogen production rates of the two films are similar at low pH_2O, but SFT1-on-SFN1 gives a much higher production rate at pH_2O = 0.49 atm, reaching 12.3 cm^3/min-cm^2.

Figure 14 shows a fracture surface and a plan view of an as-sintered SFT1 thin film on an SFN1 substrate before its hydrogen production rate was measured. The sample shown in Fig. 14 and the sample used to measure the hydrogen production rate (Fig. 13) were made in the same batch and were presumed to be identical. The SFT1 film had a thickness of ≈30 µm and appeared reasonably dense with some isolated porosity. An IPA-penetration test confirmed that the samples were dense; however, this test did not prove that the thin film alone was dense. The substrate appears (Fig. 14a) to have adequate porosity, but it might still lack interconnected porosity and prevent penetration by IPA, as was seen with other samples (Fig. 2). Hydrogen production rate measurements provide the ultimate test of a substrate's porosity, and the high production rate that was measured (12.3 cm^3/min-cm^2) indicates that the substrate contained sufficient porosity. Like other SFT1 samples tested before, the plan view of the as-sintered sample shows only rounded grains with no evidence of needle-shaped grains.

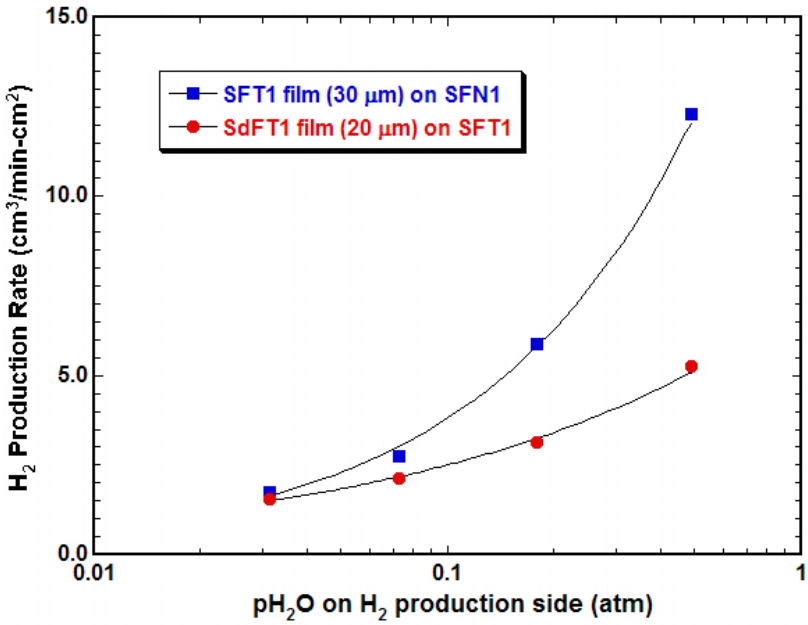

Fig. 13 Hydrogen production rates for SFT1-on-SFN1 and SdFT1-on-SFT1 samples at 900°C measured vs. pH_2O on the hydrogen-generation side with 80% H_2/balance He on the oxygen-permeate side. Inset gives film thickness.

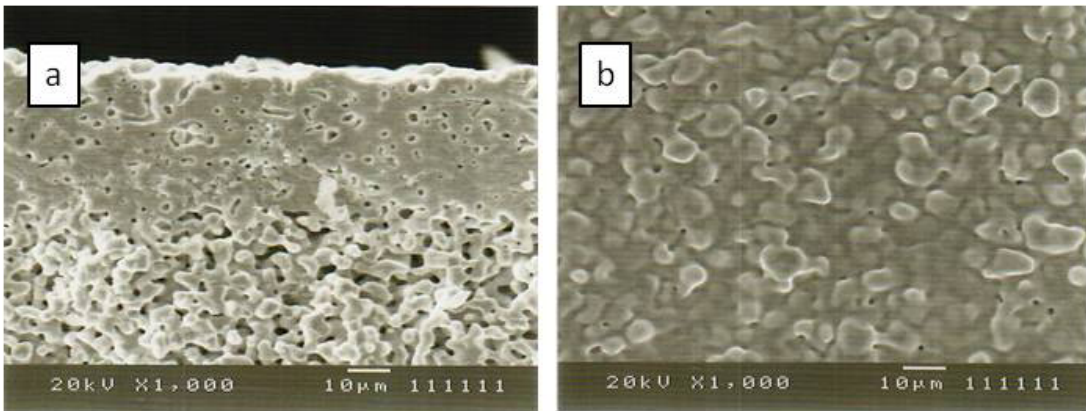

Fig. 14 Secondary electron images of SFT1 film on SFN1 substrate sintered 5 h at 1350°C in 100 ppm H_2/balance N_2: a) fracture surface and b) plan view.

Figure 15 compares the temperature dependence of the hydrogen production rate for SFT1 and SFC2 thin films. The SFC2 data were collected previously [13] with an SFC2 thin film on a porous SFC2 substrate. The SFC2 substrate was prepared from a mixture of SFC2 powder and carbon powder (20 wt.%). The SFC2 thin film was sintered at 1160°C in Ar for 7 h and had a thickness of ≈20 μm. The SFT1 thin film, on a SFN1 substrate, was sintered at 1350°C in 100 ppm H_2/balance N_2 for 5 h and had a thickness of ≈30 μm. The hydrogen production rate was measured with 80% H_2/balance He flowing on the oxygen-permeate side and humidified N_2 (pH_2O = 0.49 atm) on the hydrogen-generation side. Compared with SFC2-on-SFC-2, the hydrogen production rate for SFT1-on-SFN1 is slightly lower at high temperatures, but much higher at temperatures below 825°C, because SFT1 does not undergo a phase transition.

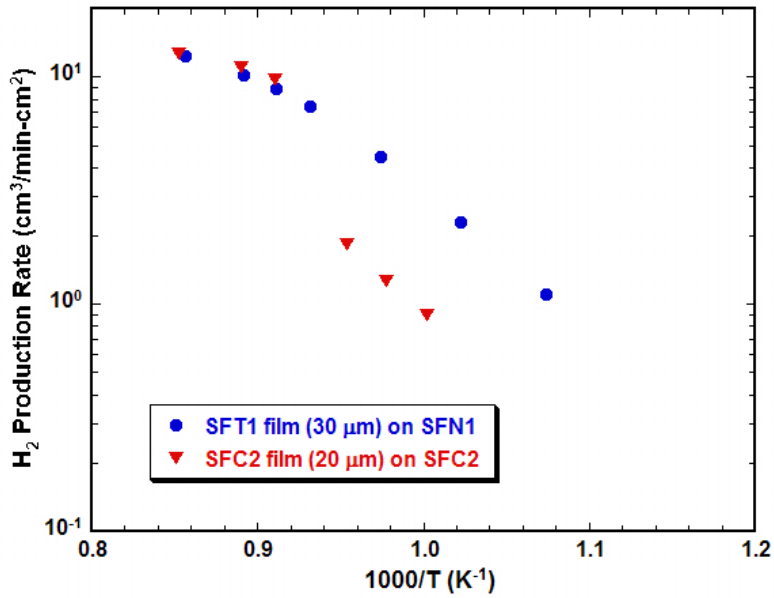

Fig. 15 Hydrogen production rates for SFT1-on-SFN1 and SFC2-on-SFC2 films measured with 80% H_2/balance He on oxygen-permeate side and pH_2O = 0.49 atm on hydrogen-generation side. Inset gives film thickness.

SFT1 thin films on SFN1 substrates were sintered at 1200-1270°C to determine whether a lower sintering temperature (<1350°C) might increase porosity in the substrates without causing a significant decrease in the density of the thin films. An increase in the substrate's porosity was expected to increase the hydrogen production rate by enhancing gas transport to and from the dense thin film. The SFT1 thin films were prepared on SFN1 substrates by the methods described above. After films were cast onto substrates, they were sintered for 5 h in ambient air at 1200-1270°C. Figure 16 shows micrographs of SFT1 films sintered for 5 h at 1200°C and 1270°C in air. After sintering, both films were tested for pinholes with IPA. The IPA quickly penetrated the film sintered at 1200°C, indicating that the film contained pinholes or interconnected porosity. Penetration by IPA was not immediately apparent with the film sintered at 1270°C, but it was noticeable after several minutes through "mud cracks."

Fracture surfaces of the SFT1-on-SFN1 samples showed that the films sintered at 1200°C and 1270°C appeared to be dense with a few isolated pores (Figs. 16a and 16c). The surface of the film sintered at 1200°C (Fig. 16b) also showed only a few tiny pores with no visible cracks, but the surface of the film sintered at 1270°C (Fig. 16d) showed fine cracks. Cracks may have appeared in the film sintered at 1270°C, but not in the film sintered at 1200°C, because the film shrank more at the higher sintering temperature. Tensile stresses would develop in the film if it shrank while the substrate did not because the temperature was too low for sintering of the substrate. The fact that SFT1-on-SFN1 substrates did not crack when sintered at 1350°C suggests that the substrate shrinks enough to prevent cracking of the film at the higher sintering temperature. The surfaces of the films also show that the films contained only round grains. The absence of needle-like grains suggests that SFT1, unlike SdFT1, is stable at the lower sintering temperature.

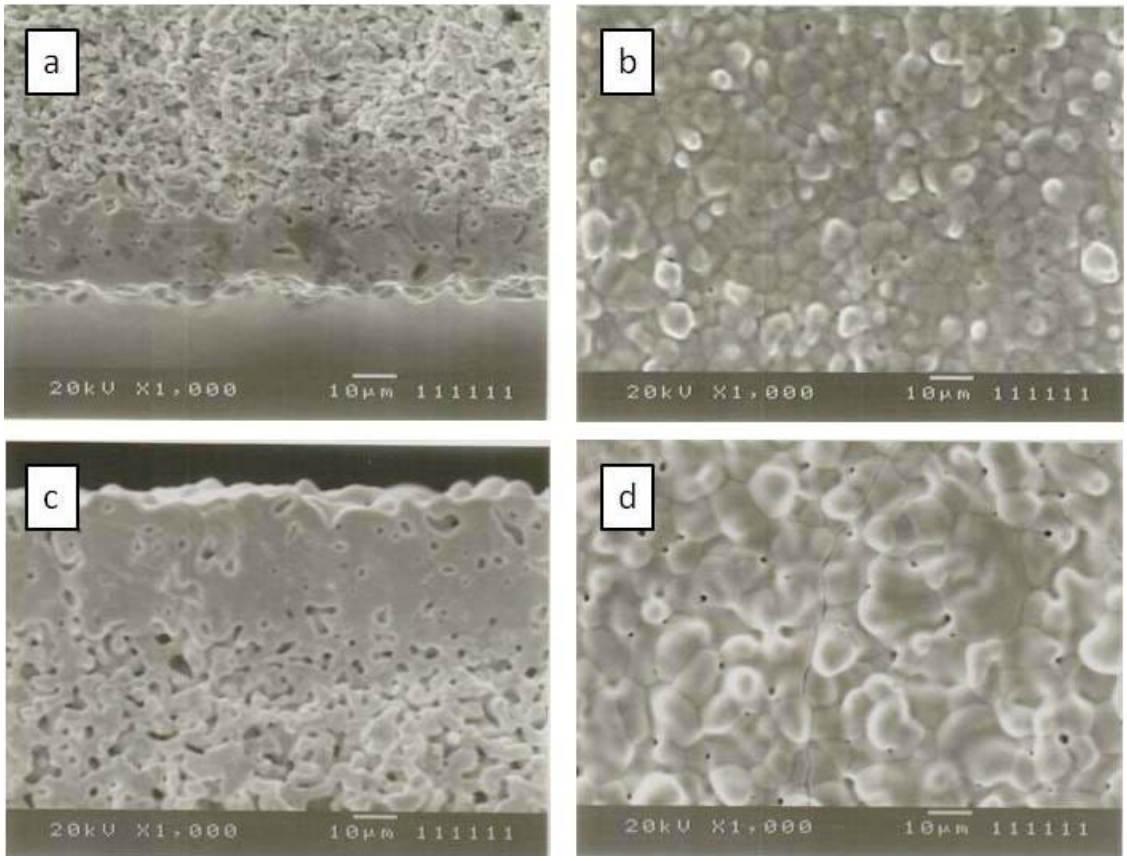

Fig. 16 Secondary electron images of SFT1 thin films on SFN1 substrates sintered for 5 h in air at 1200°C (a and b) and 1270°C (c and d).

Milestone 2. Fabricate/test thin-film OTM tubes using simulated coal combustion atmosphere to drive hydrogen production by water splitting.

To be practical, OTMs must be available in a shape with a large active area, such as tubes; therefore, we are developing methods for fabricating tubular membranes. We initially fabricated dense, self-supporting SFC2 tubes with relatively thick (≈0.7 mm) walls by pressing SFC2 powder (Praxair Specialty Ceramics) in a cold isostatic press (Engineered Pressure Systems) in a rubber mold (Trexler Rubber) with a stainless steel mandrel at 10,000-15,000 psig (680-1020 atm). Tubes were sintered at 1150°C for 10 h in flowing argon. Tubes produced by this method are typically 8-10 cm in length with an outside diameter of ≈1 cm and a membrane thickness of ≈0.7 mm. This method can be used to fabricate tubes that are open on both ends and tubes that are closed on one end.

Tubes are tested for pinholes and/or microcracks by checking for penetration of the film by IPA. In this test, the tube is filled with IPA, and the tube is examined for evidence that IPA is penetrating the film on its outer surface. Penetration of the film by even a small amount of IPA is visible as a darkening of the film and indicates that the tube contains cracks or interconnected porosity.

If an IPA-penetration test reveals no leakage, the tube's hydrogen production rate can be measured by a spring-loaded test fixture like that shown in Fig. 17. With this fixture, graphite gaskets are placed on the open ends of the tube, and the tube and gaskets are squeezed between an alumina tube and an alumina plate. If a tube passes the IPA test, it is sealed to a spring-loaded fixture and can be checked for leakage at room temperature by pressurizing the tube with 5 psi (0.3 atm) He and submerging it in IPA. If bubbling is not observed through the wall of the painted tube and is minimal at the gold ring used to seal the tube to the test fixture, the tube is placed into the reactor to measure its hydrogen production rate.

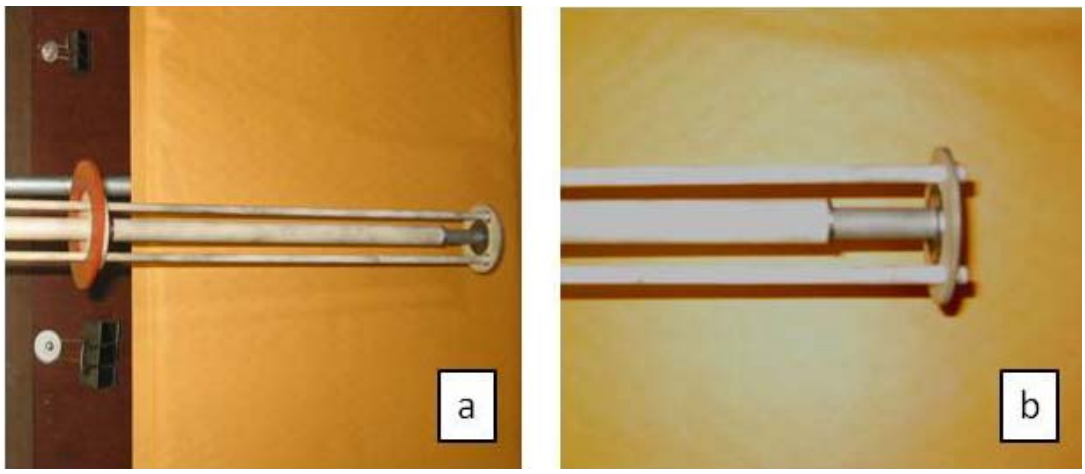

Fig. 17 Spring-loaded fixture for measuring hydrogen production rate. Tube and graphite gaskets for obtaining gas-tight seals are shown between Al_2O_3 tube and round Al_2O_3 plate at end of fixture.

To test tubular membranes, ultrahigh purity (UHP) nitrogen was bubbled through water at a fixed temperature to control the pH_2O and then was flowed over the hydrogen-generation side. Various gases (e.g., CO, 25% CO/75% CO_2, or H_2/He mixtures) were passed on the oxygen-permeate side of the membrane to drive oxygen diffusion through the OTM due to their reactivity with oxygen. The hydrogen-helium mixtures (4-80% H_2) were prepared by mixing UHP hydrogen and UHP helium with mass flow controllers. The hydrogen production rate was measured with gas flow rates of 150-400 cm^3/min at temperatures of 500-900°C. A Hewlett-Packard 6890 gas chromatograph was used to measure hydrogen concentrations on the hydrogen-generation side.

An SFC2 tube (membrane thickness, ≈0.7 mm; surface area, ≈23.4 cm^2; outside diameter, ≈1 cm; length, ≈8 cm) was prepared for testing. The tube's hydrogen production rate (Fig. 18) was measured at 900°C versus pH_2O (0.03-0.49 atm) on the hydrogen-generation side with 80% H_2/balance He flowing on the oxygen-permeate side. Measurements were made for two sets of gas flow rates: (1) 150 cm^3/min on both sides of the membrane and (2) 400 cm^3/min on the hydrogen-generation side and 200 cm^3/min on the oxygen-permeate side.

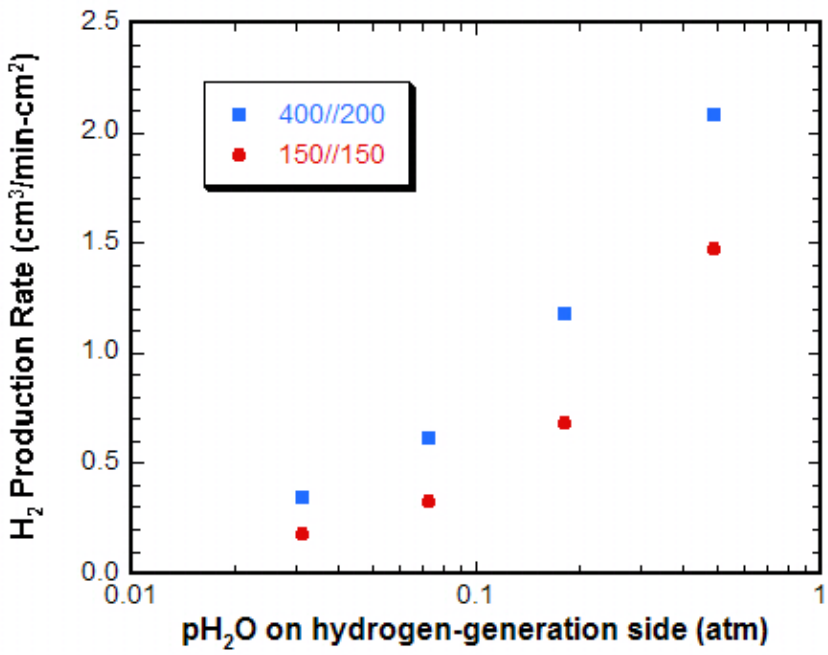

Fig. 18 Hydrogen production rate at 900°C vs. pH_2O on hydrogen-generation side of SFC2 tube with 80% H_2/He on oxygen-permeate side. Inset gives gas flow rates, e.g., 400//200 means 400 cm^3/min of N_2/H_2O on hydrogen-generation side and 200 cm^3/min of 80% H_2/He on oxygen-permeate side.

The hydrogen production rate for the tube was lower than that of a disk-type SFC2 membrane with comparable thickness under identical experimental conditions using gas flow rates of 150 cm^3/min on both sides of the membrane. With pH_2O = 0.49 atm, the tube had a hydrogen production rate of ≈1.5 cm^3/min-cm^2, whereas a 0.62-mm-thick SFC2 disk [13] had a hydrogen production rate >5 cm^3/min-cm^2. The main reason for the tube's low hydrogen production rate was believed to be concentration polarization caused by accumulation of hydrogen on the hydrogen-generation side. This hypothesis was confirmed by the increase in hydrogen production rate that resulted when the gas flow rates for the tube were increased to 400 cm^3/min on the hydrogen-generation side and 200 cm^3/min on the oxygen-permeate side.

The hydrogen production rate for the SFC2 tube was also measured over the temperature range 500-900°C with pH_2O = 0.03 atm on the hydrogen-generation side and 80% H_2/balance He on the oxygen-permeate side. The results are plotted versus inverse temperature in Fig. 19. As seen previously with SFC2 disks [12], the hydrogen production rate drops sharply for temperatures below ≈825°C as SFC2 undergoes a phase transition. Due to the low hydrogen production rate caused by the phase transition, OTMs made of SFC2 are considered unsuitable for applications at <825 °C. At temperatures >850°C, however, SFC2 shows the highest hydrogen production rate measured to date and is a good candidate for OTM applications.

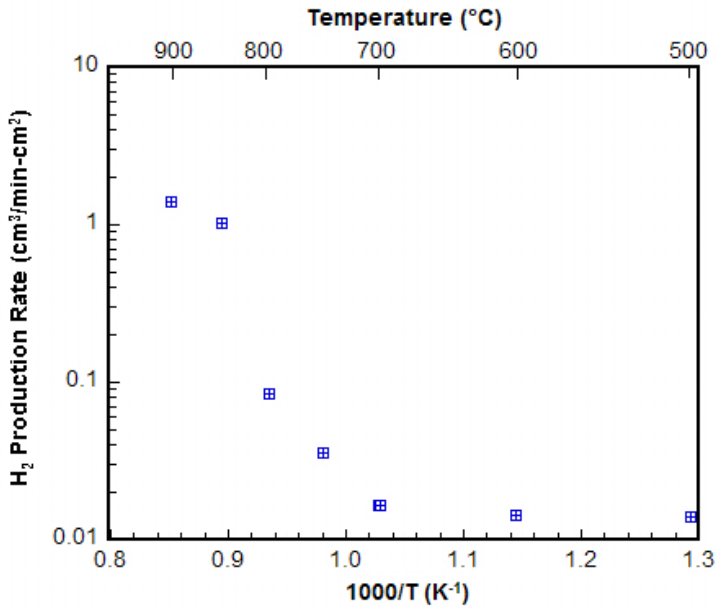

Fig. 19 Hydrogen production rate of SFC2 tube vs. inverse temperature using 80% H_2/balance He on oxygen-permeate side and humidified N_2 (pH_2O = 0.49 atm) on hydrogen-generation side.

Figure 20 shows the hydrogen production rate of the SFC2 tube versus pH_2O on the hydrogen-generation side with three different gases flowing on the oxygen-permeate side: 80% H_2/balance He, CO alone, and 25% CO/75% CO_2. The flow rate of each gas on the oxygen-permeate side was 200 ml/min. Gas on the hydrogen-generation side consisted of UHP nitrogen bubbled through water at a rate of 400 ml/min. The pH_2O on the hydrogen-generation side was fixed by controlling the temperature of the water bath. As expected, for all three gases on the oxygen-permeate side, the hydrogen production rate increased as pH_2O increased on the hydrogen-generation side. The hydrogen production rate decreased as the gas on the oxygen-permeate side was changed from 80% H_2/balance He to CO, and then to 25% CO/75% CO_2, because the change in gas decreased the driving force for oxygen diffusion through the membrane. The driving force for oxygen diffusion decreased with the change in gas because the reactivity of the gas with oxygen decreased, thereby increasing the oxygen chemical potential on the oxygen-permeate side.

Another method for fabricating tubular OTMs uses the paste-painting technique. In this approach, we first produce porous support tubes in a cold isostatic press (Engineered Pressure Systems) by pressing SFC2 powder mixed with 20 wt.% carbon with a stainless steel mandrel in a rubber mold (Trexler Rubber) at 10,000-15,000 psig (680-1020 atm). After pressing, the support tube is pre-sintered at 950°C for 5 h in ambient air to remove the carbon and provide the tube with sufficient mechanical strength for subsequent handling. The outside surface of the pre-sintered tube is painted with a paste containing SFC2 powder, and then is sintered for 10 h at 1200°C in 100 ppm H_2/N_2, giving a dense SFC2 film on a tubular porous support. Tubes made in this way are typically 8-10 cm long with a membrane thickness of 25-50 μm and an outside diameter of ≈1 cm. A typical tube made by this method is shown in Figure 21.

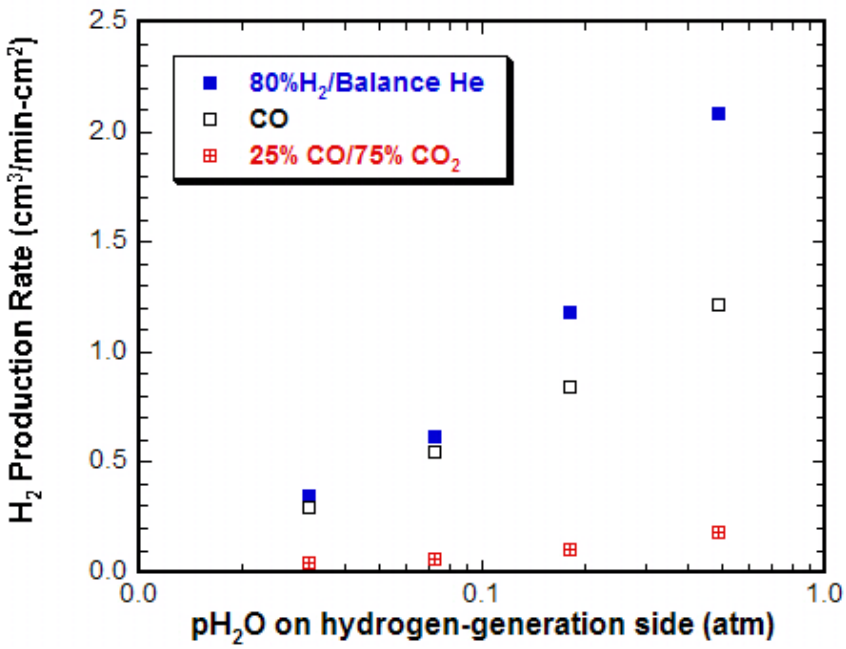

Fig. 20 Hydrogen production rates vs. pH_2O on hydrogen-generation side of SFC2 tube at 900℃ using 25% CO/75% CO_2, CO, and 80% H_2/He on oxygen-permeate side.

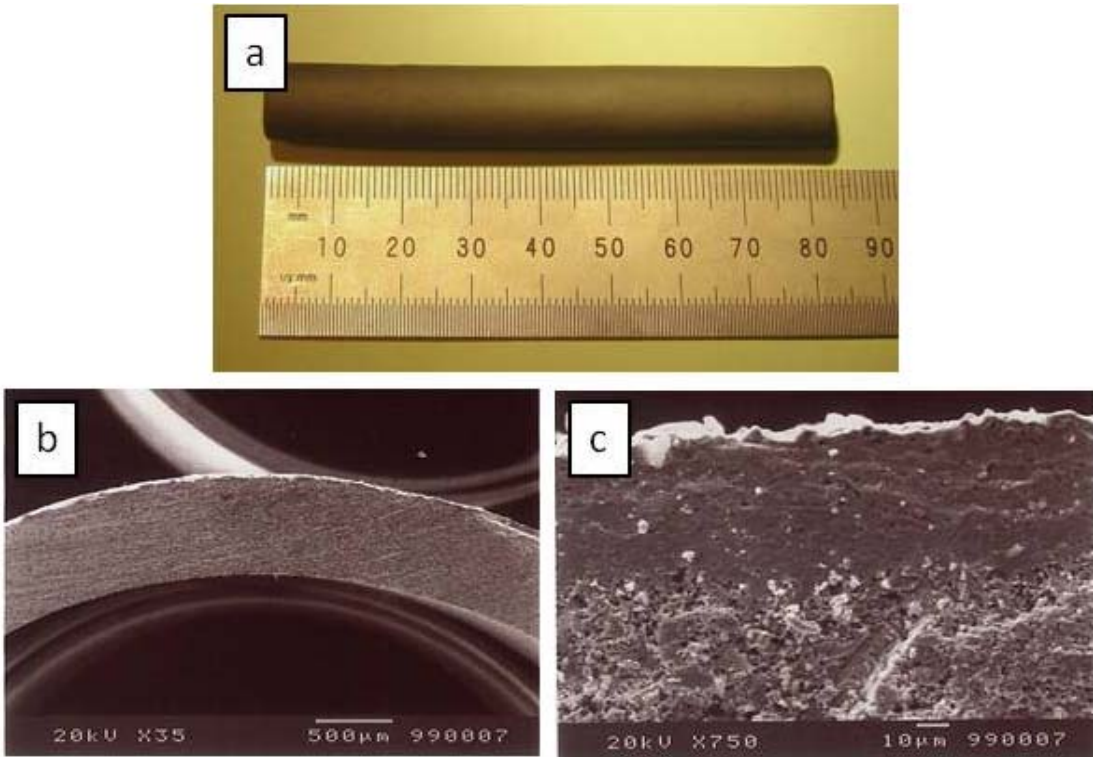

Fig. 21 Thin-film SFC2 tube made by paste-painting technique: a) photograph, b) "low" magnification cross-sectional view, and c) "high" magnification cross-sectional view.

The hydrogen production rate of a tube with SFC2 thin film (film thickness, ≈40 μm) was measured over the range 700-900°C (Fig. 22). While the measurements were made, 80% H_2/balance He was flowed on the oxygen-permeate side of the tube while humidified (pH_2O = 0.49 atm) UHP nitrogen was flowed on the steam side. Relatively high gas flow rates (500 cm^3/min) were used on the tube inside and outside to minimize concentration polarization. As a reference, the hydrogen production rates are also shown for a relatively thick (≈0.7 mm) self-supported SFC2 tube that was tested with gas flow rates of 150 cm^3/min on both sides. Both tubes show a sharp drop in hydrogen production rate at ≈825°C due to the phase transition for SFC2.

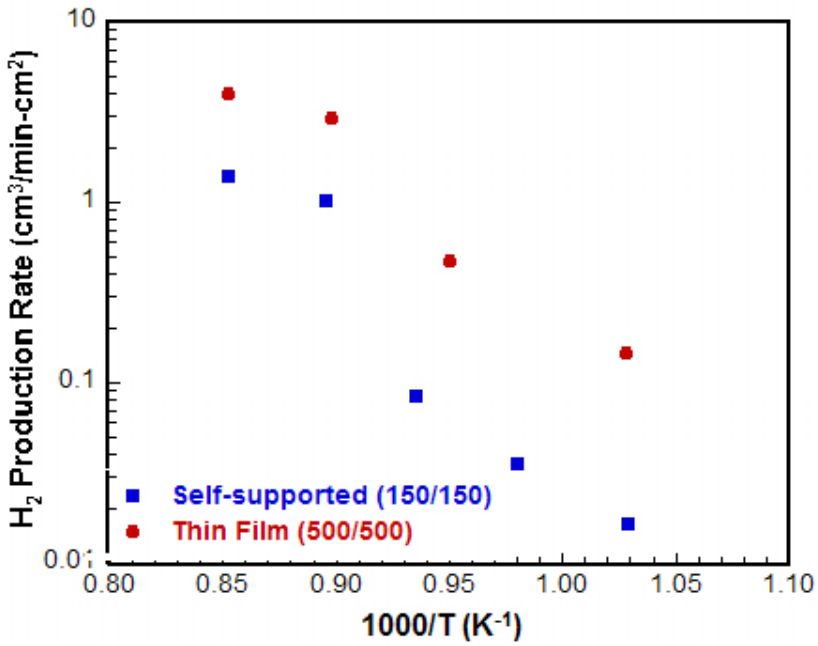

Fig. 22 Hydrogen production rate vs. temperature for thin-film and self-supported SFC2 tubes measured with 80% H_2/balance He on oxygen-permeate side and humidified N_2 (pH_2O = 0.49 atm) on steam side. Legend gives flow rates on steam and oxygen-permeate sides of tube.

Figure 23 shows the hydrogen production rate at 900°C versus pH_2O on the steam side of a tubular SFC2 thin film (thickness, ≈40 μm; surface area, ≈21.3 cm^2) and a self-supporting SFC2 tube with 80% H_2/balance He flowing on the oxygen-permeate side. As expected, the H_2 production rate increased with increasing pH_2O for both types of tube, but the thin-film tube had a higher hydrogen production rate for all values of pH_2O. With pH_2O = 0.49 atm, the thin film gave a hydrogen production rate of ≈4.3 cm^3/min-cm^2, which was about triple that of the self-supported tube (≈1.5 cm^3/min-cm^2). The higher production rate versus pH_2O (Fig. 23) and temperature (Fig. 22) for the thin-film tube can be attributed to its smaller thickness and the higher gas flow rates used for the tests. The effects of membrane thickness and gas flow rate on these data cannot be separated.

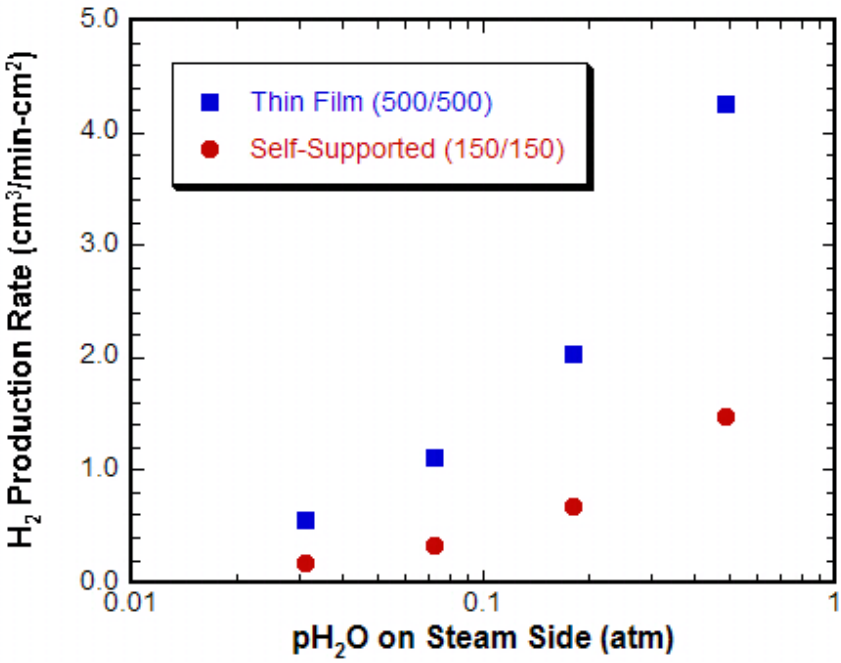

Fig. 23 Hydrogen production rate vs. pH_2O on steam side of thin-film and self-supported SFC2 tubes at 900°C measured with 80% H_2/He on oxygen-permeate side. Legend gives flow rates on steam/oxygen-permeate sides of tube.

To investigate the effect of gas flow rates, we measured the hydrogen production rate of a thin-film SFC2 tube while varying the gas flow rate on both sides of the tube. Table 1 summarizes the effect of the flow rates on the area-specific hydrogen production rate (cm^3/min-cm^2), "total" hydrogen production rate, i.e., for the entire tube (cm^3/min), and water conversion rate (the ratio of "hydrogen out" to "water in"). Figure 24 plots the effects of the flow rates on the total hydrogen production rate. During all measurements, 80% H_2/balance He was flowed on the oxygen-permeate side, while humidified N_2 was flowed on the steam side. With a fixed flow rate (150 cm^3/min) on the oxygen-permeate side, the tube hydrogen production rate increased linearly as the flow rate of N_2 (pH_2O = 0.03 atm) increased from 150 to 500 cm^3/min on the steam side. However, with the flow rate on the steam side fixed at 500 cm^3/min, the hydrogen production rate for the tube varied only slightly when the flow rate increased from 150 to 500 cm^3/min on the oxygen-permeate side. These findings indicate that the hydrogen production rate is limited more by flow rate on the steam side than the oxygen-permeate side.

Similar results were obtained with higher pH_2O (0.48 atm) on the steam side of the tube and higher flow rate (700 cm^3/min) of 80% H_2/balance He on the oxygen-permeate side. As the flow rate on the steam side was increased from 150 to 500 cm^3/min, the total hydrogen production rate increased roughly linearly. Further increasing the flow rate on the steam side to 700 cm^3/min increased the total hydrogen production rate only slightly. These results indicate that, for the tube tested here, concentration polarization effects were largely eliminated with a flow rate >500 cm^3/min on the steam side.

Table 1. Effect of gas flow rates on hydrogen production rate of tubular SFC2 thin film (film thickness ≈40 μm).

	80% H_2/He - Wet N_2 (pH_2O = 0.03 atm)			
Gas flow rate (cm^3/min)	150 - 150	150 - 300	150 - 500	500 - 500
Tube HPR[a] (cm^3/min)	5.1	7.9	11.0	11.9
Conversion rate (%)[b]	100.0	93.8	76.3	82.6
Area-specific HPR[a] (cm^3/min-cm^2)	0.24	0.37	0.52	0.56
	80% H_2/He // Wet N_2 (pH_2O = 0.48 atm)			
Gas flow rate (cm^3/min)	700 - 150	700 - 300	700 - 500	700 - 700
Tube HPR[a] (cm^3/min)	50.5	61.1	81.8	84.2
Conversion rate (%)[b]	71.3	44.7	34.3	24.7
Area-specific HPR[a] (cm^3/min-cm^2)	2.37	2.87	3.84	3.95

[a] HPR = hydrogen production rate.
[b] Conversion rate = moles H_2 out/moles H_2O in.

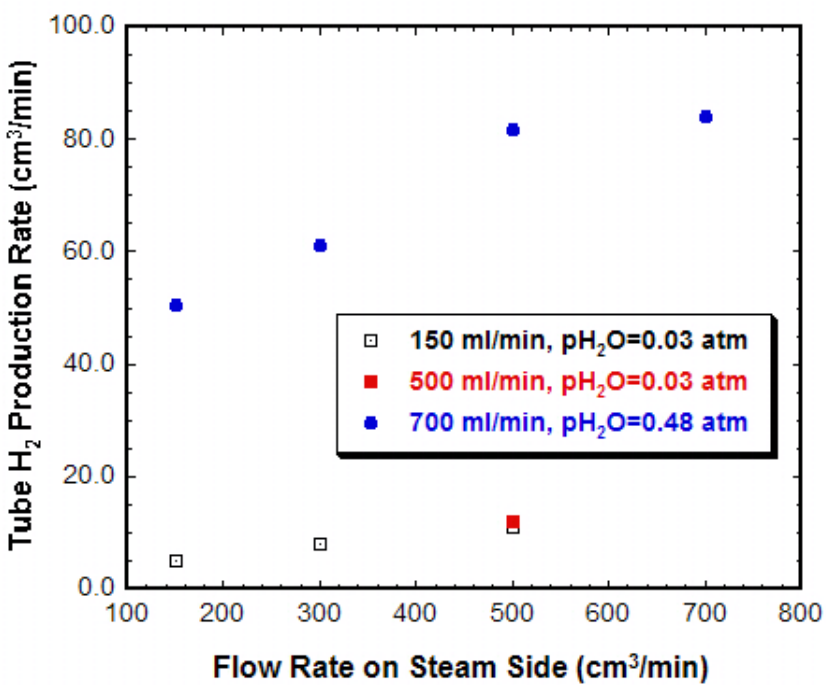

Fig. 24 Hydrogen production rate of thin-film SFC2 tube vs. flow rate of humidified N_2 on steam side. Flow rate of 80% H_2/balance He on oxygen-permeate side and pH_2O on steam side are given in legend.

Thin-film OTMs enhance hydrogen production via water dissociation, because reducing membrane thickness increases the driving force for oxygen diffusion from the hydrogen production side of the membrane; therefore, fabricating and testing thin-film tubular OTMs have been a focus of this project. By reduction of an OTM's thickness, the hydrogen production rate can be increased at high temperatures (≈900°C), or significant hydrogen production can be maintained at low temperatures (≤700°C). Significant enhancement of the hydrogen production rate was achieved with a thin-film SFC2 tube (Fig. 23), but the hydrogen production rate of SFC2 dropped dramatically at temperatures <825°C (Fig. 15). By contrast, thin-film OTMs made of SFT1 do not undergo a sharp drop in hydrogen production rate below 825°C (Fig. 15). Likewise, the hydrogen production rate of LSCF7328 does not drop sharply at low temperatures; therefore, considerable effort was made to fabricate and test LSCF7328 thin-film tubes using simulated products from coal combustion to drive hydrogen production.

Figure 25 shows a cross section of an LSCF7328 tube that was made and tested during FY 2009. The film on the surface appears dense with a thickness of 10-20 μm, and the substrate seems to have sufficient porosity. The tube's microstructure looks like that of thin-film disks that have been successfully tested, but LSCF7328 thin-film tubes tested to this point failed during testing at low temperatures (≤700°C). Without any apparent problems, the tubes survived heating to the testing temperature and heating during the sealing procedure, all under an atmosphere of inert gas. Very low leakage was measured through seals made with glass rings; however, all the tubes cracked when a reducing gas was introduced on one side of the tube. Apparently, the tubes could not withstand the stresses generated by the large gradient in oxygen chemical potential across the wall of the tube. In future tests of thin-film tubes, we will test alternative OTM compositions that might tolerate the large gradient in oxygen chemical potential during testing.

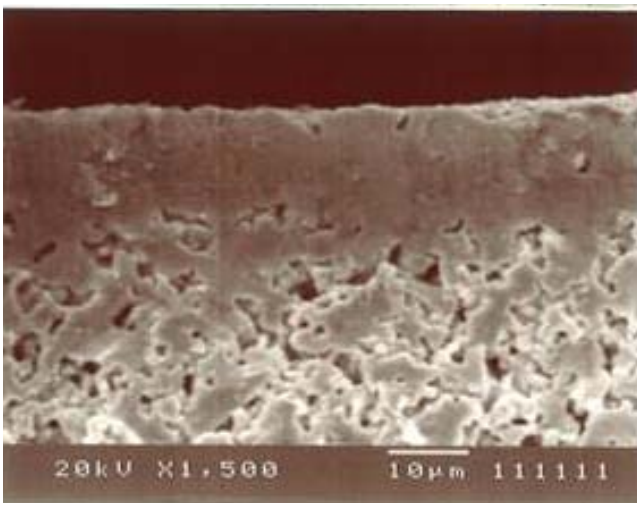

Fig. 25 Secondary electron image showing cross section of LSCF7328 thin-film tube after it cracked during attempt to measure its hydrogen production at low temperature (≤700°C).

Milestone 3. Test use of coal combustion atmosphere to drive hydrogen production by water splitting at low temperatures.

To demonstrate the concept that combustion of coal can drive hydrogen production via water dissociation, we measured the hydrogen production rate of LSCF7328 thin films in tests using CO/CO_2 gas mixtures on the oxygen-permeate side. We prepared LSCF7328 by conventional solid-state synthesis using the starting materials of La_2O_3 from Alfa Aesar (99.999%), $SrCO_3$ from Aldrich (99.9+%), CuO from Johnson Matthey (99.999%), and Fe_2O_3 from Alfa Aesar (99.99%).

Porous LSCF7328 substrates were made as supports for LSCF7328 thin films to reduce stresses caused by a mismatch in the thermal expansion coefficients of different materials. Substrates were prepared from LSCF7328 powder mixed with 20 wt.% carbon to maintain porosity during sintering. The mixture of LSCF7328 powder and carbon was ball-milled overnight in isopropyl alcohol, and then dried, uniaxially pressed into disks and fired for 10 h at 1050°C in ambient air. Thin films were prepared by painting the surface of porous LSCF7328 substrates with a slurry containing LSCF7328 powder. To prepare the slurry, LSCF7328 powder was mixed with proper amounts of a binder (polyvinyl butyral), plasticizer, and solvent (α-terpineol). After the slurry was painted onto a substrate with a brush, the sample was dried for 1 h at 80°C, and then sintered at 1100-1140°C for 10 h in air. The hydrogen production rates were determined with the LSCF7328 films (film thickness ≈22 μm) sealed to the end of an Al_2O_3 tube by using an assembly described elsewhere [14].

During hydrogen production measurements, humidified N_2 (pH_2O = 0.49 atm) was flowed over the hydrogen-generation side, while a H_2/He or CO/CO_2 mixture was flowed over the oxygen-permeate side. To fix pH_2O on the hydrogen-generation side, the N_2 was bubbled through a water bath at a fixed temperature before it was flowed over the membrane. Hydrogen on the oxygen-permeate side reacted with oxygen as it diffused through the film, thus creating a low pO_2 on the oxygen-permeate side and establishing a pO_2 gradient across the membrane. The H_2/He mixture was used on the oxygen-permeate side only as a model gas to evaluate the effects of membrane thickness, surface coating, and the porous support structure. A gas chromatograph (Hewlett-Packard 6890) was used to measure the hydrogen concentrations in the gas stream at temperatures of 600-900°C.

To demonstrate that combustion of coal can drive hydrogen production via water dissociation, we measured the hydrogen production rate of a supported LSCF7328 thin film (film thickness ≈22 μm) while flowing humidified N_2 (pH_2O = 0.49 atm) on the hydrogen-generation side and simulated coal combustion products (CO/CO_2 mixtures) on the oxygen-permeate side. To compare the supported LSCF7328 film's performance to that of other LSCF7328 films, its hydrogen production was first measured while flowing 80% H_2/balance He on the oxygen-permeate side. The hydrogen production rate at 900°C (9.0 cm^3/min-cm^2) was close to the value (9.8 cm^3/min-cm^2) for another LSCF7328 film with similar thickness and tested under identical conditions, indicating that the properties of the LSCF7328 films are reproducible.

The H_2 production rate for the LSCF7328 thin film is plotted (Fig. 26) versus the CO concentration in the simulated coal combustion atmosphere on the oxygen-permeate side. The CO concentration was balanced with either CO_2 or He for the measurements at 600 and 900°C, but was balanced with only CO_2 for the measurements at 700 and 800°C. Dissociation of CO_2 increases the pO_2 in CO/CO_2 mixtures relative to CO/He mixtures with the same nominal CO concentration; consequently, the driving force for oxygen diffusion is smaller with a CO/CO_2 mixture on the oxygen-permeate side of the membrane. As a result, CO/CO_2 mixtures on the oxygen-permeate side give a smaller hydrogen production rate than do CO/He mixtures with the same nominal CO concentration.

Figure 27 shows the hydrogen production rate of an LSCF7328 thin-film membrane versus the CO concentration on its oxygen-permeate side. With CO (99.5% purity) on the oxygen-permeate side, a hydrogen production rate of ≈4.7 $cm^3/min\text{-}cm^2$ was measured at 900°C, showing that hydrogen can be produced at a significant rate when gases from coal combustion are used to drive the dissociation of water. As the CO concentration decreased on the oxygen-permeate side, the pO_2 increased, causing the driving force for oxygen diffusion from the hydrogen-generation side to decrease. As a result, the hydrogen production rate decreased as the CO concentration decreased. Because oxygen diffusion is thermally activated, the hydrogen production rate also decreased as temperature decreased. The CO concentration had a similar effect on the hydrogen production rate of an SFC2 tubular membrane (Fig. 20).

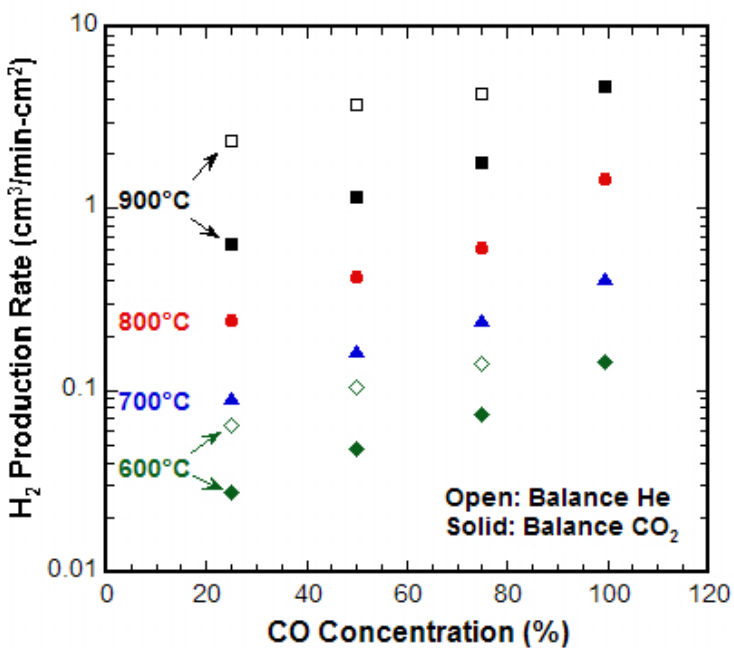

Fig. 26 Hydrogen production rate for LSCF7328 film on porous LSCF7328 substrate vs. carbon monoxide concentration on oxygen-permeate side with balance of He (open symbols) or CO_2 (solid symbols). Humidified N_2 (pH_2O = 0.49 atm) flowed on hydrogen-generation side.

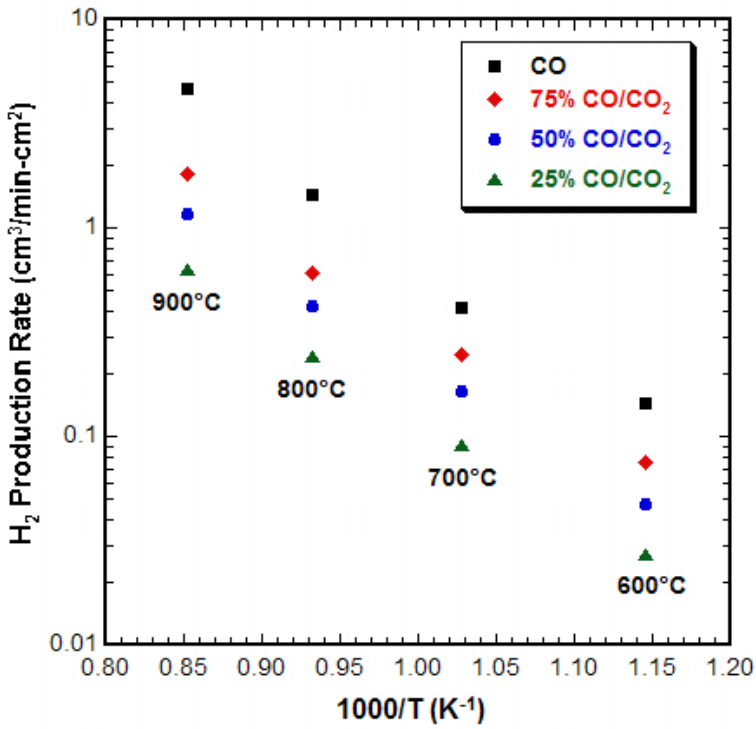

Fig. 27 Hydrogen production rate of LSCF7328 film on porous LSCF7328 substrate, measured with various CO/CO_2 gas mixtures on oxygen-permeate side. Humidified N_2 (pH_2O = 0.49 atm) flowed on hydrogen-generation side.

V. FUTURE WORK

We will continue efforts to develop new OTM materials for producing hydrogen via coal/coal gas-assisted water splitting. In these efforts, we will investigate new membrane compositions and apply methods described in this report to enhance the hydrogen production rate of the OTMs being developed. Based on the principles of solid-state chemistry, we will prepare and test novel materials thought to have potential for high hydrogen production rates. To increase the hydrogen production rates of existing OTM materials, we will continue to improve methods for reproducibly fabricating membranes with thickness < ≈25 μm, and we will coat membranes with porous layers, working to optimize the microstructural features of the porous layers, such as porosity and pore size. When the hydrogen production rate is significantly influenced by sintering conditions, we will optimize the sintering process to enhance hydrogen production.

We will fabricate and test tubular thin-film OTMs in FY2010 to demonstrate that OTMs with a significant hydrogen production rate are practical for large-scale industrial applications. Tubes are practical for large-scale industrial processes due to their large active area and the relative ease of their fabrication and gas manifolding. To enhance the hydrogen production rates of tubular thin films, we will develop methods to coat both the inside and outside of the tube with porous layers.

Thin-film OTM tubes will be used to demonstrate that the products from coal combustion can drive hydrogen production via water dissociation. In this concept, coal is combusted on one side of an OTM while hydrogen is produced on the other side via water splitting. This concept increases process efficiency by reducing the number of steps needed to produce hydrogen from coal. In this concept, the hydrogen produced is physically separated from carbon dioxide and all other impurities; therefore, hydrogen purification is simpler and more cost-effective. Gas separation costs would be reduced because the OTM contains no precious metals. Because coal combustion is exothermic, it would supply heat that is required for water splitting. In addition, the CO_2-rich waste stream from the proposed process would be ideal for sequestration. During FY 2010, we will use CO/CO_2 gas mixtures to test the feasibility of this concept at low temperatures (≤700°C). The concept was demonstrated at low temperatures using LSCF7328 thin-film disks with CO/CO_2 gas mixtures simulating a coal combustion atmosphere, but tests with LSCF7328 thin-film tubes failed when the tubes cracked. To prevent cracks in LSCF7328 thin-film tubes during tests at low temperatures, modifications will be made in the processing and/or testing of these tubes. If cracking of LSCF7328 thin-film tubes appears to be unavoidable, alternative OTM compositions will be tested.

Good chemical stability is a critical requirement for OTMs due to the high temperatures and corrosive environments they will encounter; therefore, we will continue evaluating the chemical stability of OTMs in FY 2010. We will test the chemical and mechanical stability of OTMs in longer (up to ≈1000 h) exposures to industrially useful conditions, e.g., the atmospheres and temperatures that are typical for coal combustion and coal gasification. We will study the effect of syngas components on the hydrogen production rate of OTMs in the presence of H_2S and without H_2S. To assess the extent and course of reaction between the membrane and the atmosphere, the microstructure of membranes will be examined before and after exposures to industrial conditions.

We will evaluate process issues and economics as technical progress warrants. As directed by NETL's program managers, we will make contacts and hold discussions with potential collaborators. We will work with NETL's in-house R&D team and their Systems Engineering group to validate the process concept and assess the techno-economics of using OTMs to produce hydrogen by water splitting. We will provide technical input and engineering data to the NETL team to develop models for process viability and for thermal management studies.

PUBLICATIONS, PATENTS, AND PRESENTATIONS

Hydrogen Production by High-Temperature Water Splitting Using Mixed Oxygen Ion-Electron Conducting Membranes, Proc. 201st Electrochem. Soc. Mtg., Philadelphia, PA, May 12-17, 2002.

Method for Generating Hydrogen by Catalytic Decomposition of Water, U.S. Patent 6,468,499, Oct. 22, 2002.

Hydrogen Production by Water Splitting Using Mixed Conducting Membranes, Proc. National Hydrogen Assoc. 14th Annual U.S. Hydrogen Meeting, Washington, DC, March 4-6, 2003.

Hydrogen Production by Water Dissociation Using Mixed-Conducting Membranes, presented at 225th Amer. Chem. Soc. Natl. Mtg., Fuel Chemistry Div., New Orleans, March 23-27, 2003.

Hydrogen Production by Water Dissociation Using Oxygen-Permeable Cermet Membranes, presented at 105th Ann. Mtg. of Amer. Ceram. Soc., Nashville, April 27-30, 2003.

Hydrogen Production by Water Dissociation Using Mixed Conducting Membranes, presented at Second Information Exchange Meeting on Nuclear Production of Hydrogen, Argonne Natl. Lab., Oct. 2-3, 2003.

Use of Mixed Conducting Membranes to Produce Hydrogen by Water Dissociation, Intl. J. of Hydrogen Energy, 29, 291-296 (2004).

Hydrogen Production from Water Splitting Using Mixed Oxygen Ion-Electron Conducting Membranes, U.S. Patent 6,726,893, Apr. 27, 2004.

Hydrogen Production by Water Dissociation Using Mixed-Conducting Ceramic Membranes, Proc. of National Hydrogen Association's 15th Annual U.S. Hydrogen Energy Conf., Los Angeles, CA, April 27-30, 2004.

Hydrogen Production from Water Using Mixed-Conducting Ceramic Membranes, presented at 15th World Hydrogen Energy Conf., Yokohama, Japan, June 27-July 2, 2004.

Development of Dense Ceramic Membranes for Hydrogen Production and Separation, presented at American Soc. for Materials--Annual Materials Solution Conf., Columbus, OH, Oct. 18-21, 2004.

Hydrogen Production by Water Splitting Using Dense Thin-Film Cermet Membranes, presented at Fall Meeting of Materials Research Society, Boston, Nov. 28-Dec. 2, 2005.

Hydrogen Production by Water Dissociation Using Mixed Oxygen Ion-Electron Conducting Membranes, presented at Electrochem. Soc. 2005 Fall Mtg., Los Angeles, Oct. 16-21, 2005.

Hydrogen Production by Water Dissociation Using Mixed-Conducting Dense Ceramic Membranes, invited presentation at Amer. Chem. Soc. 231st Natl. Mtg., Atlanta, March 26-30, 2006.

Hydrogen Production by High-Temperature Water Splitting Using Electron-Conducting Membranes, U.S. Patent 7,087,211, Aug. 8, 2006.

Mixed-Conducting Membranes for Hydrogen Production and Separation, presented at 2006 MRS Fall Meeting, Boston, MA, Nov. 27 - Dec 1, 2006.

Hydrogen Production by Water Dissociation Using Mixed-Conducting Dense Ceramic Membranes, Intl. J. of Hydrogen Energy, 32, 451 (2007).

Reforming of Natural Gas via Water Splitting Using Dense Ceramic Membranes, presented at Natl. Hydrogen Assoc. Meeting, San Antonio, TX, March 19-22, 2007.

Hydrogen Production by Water Splitting Using Mixed Ionic-Electronic Conducting Membranes, presented at 211th Meeting of Electrochem. Soc., Chicago, IL, May 6-10, 2007.

Hydrogen Production by Reforming of Natural Gas via Water Splitting using Dense Ceramic Membranes, presented at Intl. Symposium on Materials Issues in a Hydrogen Economy, Richmond, VA, Nov. 12-15, 2007.

Hydrogen Production by Water Dissociation Using Oxygen Transport Membranes, presented at 213th Electrochemical Soc. Meeting, Phoenix, Arizona, May 18-23, 2008.

$La_{0.7}Sr_{0.3}Cu_{0.2}Fe_{0.8}O_{3-x}$ as Oxygen Transport Membrane for Producing Hydrogen via Water Splitting, presented at 213th Electrochemical Soc. Meeting, Phoenix, Arizona, May 18-23, 2008.

Hydrogen Production from Fossil and Renewable Sources using an Oxygen Transport Membrane, International Journal of Hydrogen Energy, 2010, in press.

REFERENCES

[1] U. Balachandran et al., Argonne National Laboratory Hydrogen Separation Membranes--Annual Report for FY 2003.

[2] U. Balachandran et al., Argonne National Laboratory Hydrogen Separation Membranes--Annual Report for FY 2002.

[3] S. Ihara, Bull. Electrotech. Lab., **41**, 259-280 (1977).

[4] B. Ma, et al., Ceram. Trans., **73**, 169-177 (1997).

[5] P. S. Maiya, et al., Solid State Ionics, **99**, 1-7 (1997).

[6] L. Qiu, et al., Solid State Ionics, **76**, 321-329 (1995).

[7] T. H. Lee, et al., Solid State Ionics, **100**, 77-85 (1997).

[8] H. Naito and H. Arashi, Solid State Ionics, **79**, 366-370 (1995).

[9] U. Balachandran et al., Argonne National Laboratory Hydrogen Separation Membranes--Annual Report for FY 2008.

[10] J.R Jurado, F.M. Figueiredo, B. Gharbage, and J.R. Frade, Solid State Ionics, **118**, 89 (1999).

[11] T. H. Lee, S. E. Dorris, and U. Balachandran, Solid State Ionics, **176,** 1479 (2005).

[12] U. Balachandran, et al., Hydrogen Production by Water Dissociation Using Ceramic Membranes--Annual Report for FY 2004, Argonne National Laboratory.

[13] U. Balachandran, et al., Hydrogen Production by Water Dissociation Using Ceramic Membranes--Annual Report for FY 2007, Argonne National Laboratory.

[14] U. Balachandran, et al., Hydrogen Production by Water Dissociation Using Ceramic Membranes--Annual Report for FY 2000, Argonne National Laboratory.

Energy Systems Division
Argonne National Laboratory
9700 South Cass Avenue, Bldg. 212
Argonne, IL 60439-4838

www.anl.gov

Argonne National Laboraory is a U.S. Department of Energy
laboratory managed by UChicago Argonne, LLC